Remote Sensing of Environment 241 (2020) 111716

Contents lists available at ScienceDirect

Remote Sensing of Environment

journal homepage: www.elsevier.com/locate/rse

Deep learning in environmental remote sensing: Achievements and challenges

Qiangqiang Yuan[a,d,f], Huanfeng Shen[b,d,e,*], Tongwen Li[b], Zhiwei Li[b], Shuwen Li[a], Yun Jiang[b], Hongzhang Xu[a], Weiwei Tan[c], Qianqian Yang[a], Jiwen Wang[a], Jianhao Gao[a], Liangpei Zhang[c,d]

[a] School of Geodesy and Geomatics, Wuhan University, Wuhan, China
[b] School of Resource and Environmental Sciences, Wuhan University, Wuhan, China
[c] The State Key Laboratory of Information Engineering in Surveying, Mapping and Remote Sensing, Wuhan University, Wuhan, China
[d] Collaborative Innovation Center of Geospatial Technology, Wuhan, China
[e] The Key Laboratory of Geographic Information System, Ministry of Education, Wuhan University, Wuhan, China
[f] Key Laboratory of Geospace Environment and Geodesy, Ministry of Education, Wuhan University, Wuhan, China

ARTICLE INFO

Edited by Jing M. Chen

Keywords:
Environmental remote sensing
Deep learning
Parameter retrieval
Neural network

ABSTRACT

Various forms of machine learning (ML) methods have historically played a valuable role in environmental remote sensing research. With an increasing amount of "big data" from earth observation and rapid advances in ML, increasing opportunities for novel methods have emerged to aid in earth environmental monitoring. Over the last decade, a typical and state-of-the-art ML framework named deep learning (DL), which is developed from the traditional neural network (NN), has outperformed traditional models with considerable improvement in performance. Substantial progress in developing a DL methodology for a variety of earth science applications has been observed. Therefore, this review will concentrate on the use of the traditional NN and DL methods to advance the environmental remote sensing process. First, the potential of DL in environmental remote sensing, including land cover mapping, environmental parameter retrieval, data fusion and downscaling, and information reconstruction and prediction, will be analyzed. A typical network structure will then be introduced. Afterward, the applications of DL environmental monitoring in the atmosphere, vegetation, hydrology, air and land surface temperature, evapotranspiration, solar radiation, and ocean color are specifically reviewed. Finally, challenges and future perspectives will be comprehensively analyzed and discussed.

1. Introduction

The earth's environmental deterioration, which is caused by human behavior and is continuously aggravating, has become the primary problem hindering further developments of global changes. The lack of resources and environmental deterioration are no longer exclusive phenomena in specific regions. In the last 50 years, space information technology, especially satellite remote sensing technology, has provided advanced detection and research means for the investigation of the earth's resources, the monitoring of local and regional environmental changes, and even the study of global changes, with the advantages of being macro, comprehensive, fast, dynamic, and accurate (Overpeck et al., 2011; Yang et al., 2013).

Remote sensing data are mainly used for environmental parameter monitoring based on physical models (Liang, 2005). Although physical models can effectively express the formation process from environmental parameters to remote sensing observations, these models are largely dependent on the prior knowledge of the model parameters. Such knowledge often has large uncertainty due to the high complexity of the physical process and varies in different periods and regions, which tends to result in the limited accuracy of environmental remote sensing. Therefore, various forms of data-driven machine learning (ML) methods have historically played a valuable role in environmental remote sensing. With the increasing availability of "earth big data" and rapid advances in ML, increasing opportunities for novel methods in earth environmental monitoring have emerged. Deep learning (DL), which has attracted broad attention in recent years, is a potential tool focusing on large-size and deep artificial neural networks. The DL models can accurately approximate the complicated nonlinear relationship between environmental parameters owing to multi-layer learning (LeCun et al., 2015; Bengio et al., 2013), which help capture the potential association between environmental variables for remote

* Corresponding author at: School of Resource and Environmental Sciences, Wuhan University, Wuhan, China.
E-mail address: shenhf@whu.edu.cn (H. Shen).

https://doi.org/10.1016/j.rse.2020.111716
Received 1 March 2019; Received in revised form 17 January 2020; Accepted 8 February 2020
Available online 27 February 2020
0034-4257/

sensing retrieval, fusion, downscaling, and so forth; besides, DL has reported great superiorities in multiscale and multilevel feature extraction from remote sensing images and combining these features from low level to high level (Zhang et al., 2016b), thus contributing to a high performance in image processing and classification problems. As a result, DL models have outperformed traditional models with substantial improvement in earth environmental monitoring with remote sensing data (Reichstein et al., 2019).

Although several review papers on DL in remote sensing have been published, these papers mainly focus on the preprocessing and classification problem from the image processing perspective (Ball et al., 2017; Ma et al., 2019; Zhang et al., 2016b; Zhu et al., 2017) or the DL-based quantitative remote sensing analysis in a specific field (for instance, hydrology (Marçais and de Dreuzy, 2017; Shen, 2018; Shen et al., 2018a) and atmospheric aerosol (Di Noia and Hasekamp, 2018)). The comprehensive quantitative remote sensing analysis using DL has been poorly explored. The traditional NN and DL models have been used in earth environmental monitoring, and numerous works have been published in recent decades (Aires et al., 2005; Aires et al., 2001; Chlingaryan et al., 2018; Li et al., 2017a; Zhang et al., 2018b). Therefore, this review will concentrate on the DL applications to advance the environmental remote sensing process. The main outline (Fig. 1) of this paper is as follows. (1) The DL potential for environmental remote sensing, including land cover mapping, environmental parameter retrieval, data fusion and downscaling, and missing information reconstruction and prediction, will be comprehensively analyzed. (2) Some popular DL network architectures and their use for remote sensing applications will be introduced. (3) Some key areas in environmental remote sensing, in which traditional NN and DL have been used, will be reviewed. These areas include land cover mapping, atmosphere parameter estimation, land surface quantitative retrieval, and hydrological parameter sensing. (4) Finally, some new insights into the ways by which DL can be efficiently driven for environmental remote sensing will be provided. For example, this study will provide the method of combining the physical and DL models. The incorporation of the geographical laws into intelligent DL architecture is also another potential research direction. The DL-based quantitative retrieval is largely dependent on the training samples. Thus, this review will also provide knowledge on the effective use of DL in the limited sample condition.

The remainder of this paper is arranged as follows. Section 2 discusses the use of DL for environmental remote sensing. Section 3 analyzes some popular network structures and the roles of various networks for different data processing tasks. Section 4 provides a comprehensive review of the applications of the traditional NN and DL in environmental remote sensing, including land cover mapping and quantitative parameter retrieval. Section 5 discusses the potential research directions and future perspectives. Finally, Section 6 summarizes the conclusions.

2. What can DL do for environmental remote sensing?

The DL applications in remotely sensed images are different from those in natural images, the remotely sensed images usually have more complicated and diverse patterns, as well as richer spatio–temporal–spectral information that can be used, thus higher requirements are imposed on the processing methods of remotely sensed images. Thanks to the strong ability of DL in feature representation, DL has been introduced into environmental remote sensing and applied in many aspects, including land cover mapping, environmental parameter retrieval, data fusion and downscaling, and information construction and prediction. The detailed applications of DL in environmental remote sensing are as follows.

2.1. Land cover mapping

Land cover mapping from remote sensing imagery relies on image classification. Traditional classification methods categorize images based on different spatial units, including pixels, moving windows, objects, and scenes (Blaschke, 2010; Ma et al., 2017; Zhang et al., 2018b). However, distinguishing the complex land structures or patterns by using a limited number of rules is often difficult because traditional methods only involve low-level features in spectral and spatial domains in classification. Thus, classification approaches using a huge number of features at high levels are desirable. DL has been recently introduced to land cover mapping and obtained optimal results due to its superiorities in multiscale and multilevel feature extraction (Huang et al., 2018; Scott et al., 2017b; Zhang et al., 2019). Compared with the traditional rule-based and ML methods, the DL-based classification method has significant advantages in terms of classification accuracy, especially in complex urban areas. With the requirements of land cover mapping from high-resolution and even very-high-resolution satellite imageries, DL-based land-cover classification methods have shown their potentials in current applications.

2.2. Environmental parameter retrieval

Remote sensing retrieval of environmental parameters is often achieved by physical models, which are grounded in systematic

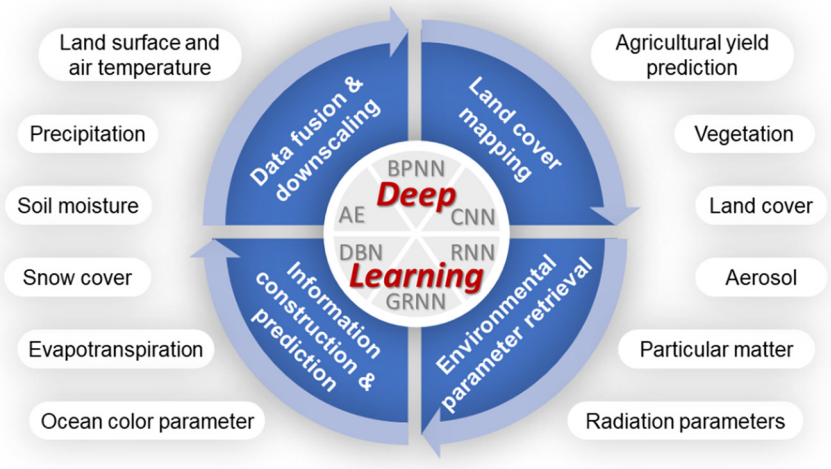

Fig. 1. Main outline of this work.

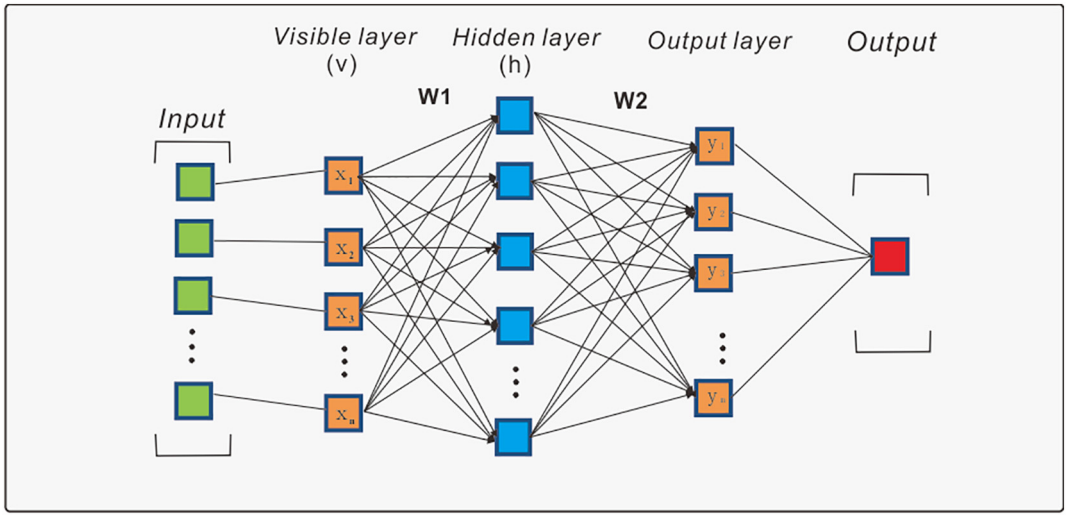

Fig. 2. BPNN structure.

physical theories and mechanisms. However, the physical processes are highly complicated and involve numerous model parameters. Furthermore, a sound physical model is yet to be developed for some environmental phenomena. Given this fact, DL has a good opportunity to retrieve environmental parameters. First, DL can simulate or simplify the physical models for environmental parameter retrieval. The hugely complex computation is necessary for physical models, and DL can be used for the forward simulation of physical models, in part or in whole, owing to its considerable simulation capability. Thus, the retrieval process of environmental parameters can be simplified. Second, DL is effective for establishing the statistical relationship between remote sensing observations and in-situ environmental parameters owing to its capacity of approximating complex relationships (LeCun et al., 2015). This avoids the complicated physical models and can obtain a comparable performance. Perhaps more importantly, DL can provide an alternative and feasible way for environmental parameter retrieval in certain environmental phenomena with a lack of sound physical models.

2.3. Data fusion and downscaling

Remote sensing satellite sensors feature a tradeoff among the spatial, temporal, and spectral resolutions. Data fusion, which merges the complementary information, is an effective way to obtain high spatio–temporal–spectral resolution data (Shen et al., 2016). The fusion of various data indicates the establishment of a complicated spatio–temporal–spectral relationship for different input data. This process is similar to data downscaling, which establishes a statistical association between the coarse-resolution parameter and high-resolution auxiliary data (Peng et al., 2017). Therefore, the key issue for data fusion and downscaling is how to build the relationships between various data, which is exactly what DL is good at (LeCun et al., 2015). DL can capture the abstract features of remote sensing observations and learn the potential associations between different observations through multilayer learning. Hence, the complicated relationship for data fusion and downscaling can be comprehensively represented by DL. In addition, DL establishes the relationship by extracting abstract features from data samples, which are less influenced by the observation properties, such as sensor type and spatial scale. Thus, robust relationships can be established in DL models.

2.4. Information construction and prediction

Missing information in remote sensing data, which are caused by dead lines, gaps, and cloud cover, are common (Shen et al., 2015). To date, various methods have been developed for the reconstruction of missing information in remote sensing data for different tasks. These methods obtained satisfactory recovery results, such as gap filling (Zeng et al., 2013), cloud removal (Cheng et al., 2014), normalized difference vegetation index (NDVI), and land surface temperature (LST) reconstruction (Yang et al., 2015; Zeng et al., 2018). However, most reconstruction methods are based on linear models and can only be used under limited conditions. This limitation contributes to the difficulty in handling complex surfaces and large missing areas. Convolutional NNs (CNNs) have been recently successfully applied to deal with missing data prediction (Das and Ghosh, 2017), gap filling and cloud removal (Zhang et al., 2018c), and LST reconstruction (Wu et al., 2019) because of the strong nonlinear representation capability of the DL model and acquired state-of-the-art results. This notion indicates the potential of DL for missing information reconstruction and prediction in remote sensing data.

3. Basic DL framework

Although the NN has good universality, a single network framework cannot address all problems. To date, many different NN frameworks have been developed to deal with various types of problems, thereby demonstrating the importance of network frameworks. The back-propagation NN (BPNN) and generalized regression NN (GRNN) are two typical examples in the traditional neuron network framework. To date, the four mainstream DL architectures include the autoencoder (AE), CNN, deep belief network (DBN), and recurrent NN (RNN). The following sections will further discuss each of these architectures.

3.1. BPNN

BPNN is one of the basic NNs. In BPNN (Fig. 2), at least one hidden layer is present between one input and one output layer. Several nodes or neurons can be found in each layer. The BPNN algorithm mainly comprises forward and backward propagation: the neurons in the input layer are passed through each hidden layer successively to finally reach the output layer. If the expected results are not obtained in the output layer, then the errors are back-propagated to update the neuron weights of each hidden layer iteratively and finally minimize them.

BPNN, which is one of the popular algorithms of ML, has been used in most aspects of remote sensing research. Li et al. (2007b) recently established a hyperspectral retrieval model of soybean leaf area index (LAI) estimation by BPNN. This model considerably improved accuracy

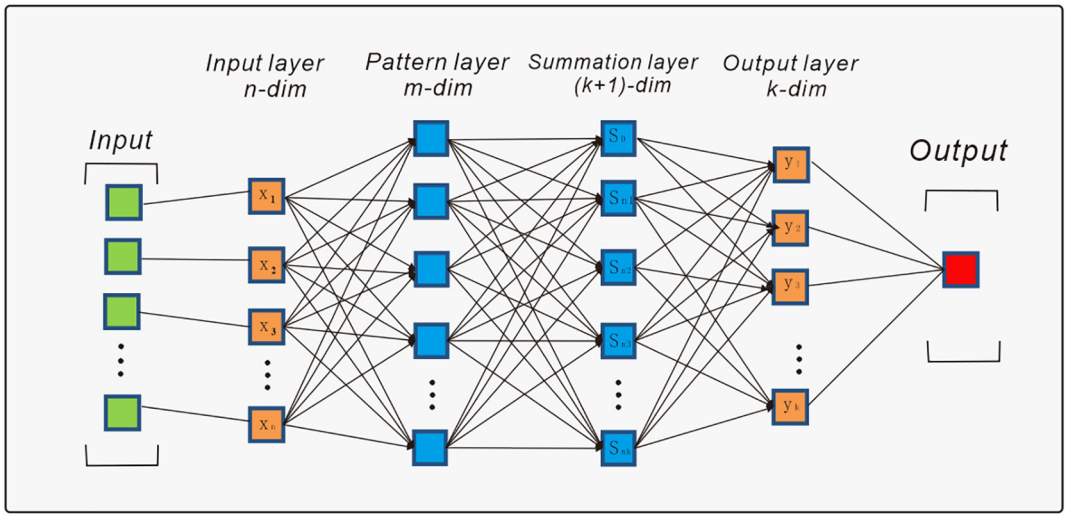

Fig. 3. GRNN structure.

compared with traditional regression models. Yang et al. (2011) attempted to interpolate the NDVI maps with the BPNN interpolation algorithm and results confirmed its advantage compared with Kriging interpolation. Liang et al. (2011) compensated for the sample temperature with a principal component analysis BPNN (PCA-BPNN) model, which significantly promoted the analytical precision. BPNN is generally widely used in multi-parameter retrieval tasks. However, further BPNN applications are constrained because of two drawbacks derived from its nature: on the one hand, BPNN slowly converges during the training process; on the other hand, BPNN is sensitive to the initial network weights, and different initial weights may facilitate the model convergence to different local minimum values.

3.2. GRNN

GRNN is a special type of radial basis NN, which usually comprises four layers: input, pattern, summation, and output layers (Fig. 3). Each GRNN layer contains several neurons. The sample dimension is the number of neurons in the input layer. The Gaussian function is calculated in the pattern layer, and the number of neurons is the number of training samples. The summation layer neurons are divided into two parts. The first neuron outputs the arithmetic sum of the pattern layer, and the rest of the k nodes output the weighted sum of the pattern layer. The labels' dimension k is the number of neurons in the output layer. Each neuron in the output layer is equal to the corresponding neuron of the summation layer divided by the first neuron in the summation layer. Specifically, GRNN is a complete forward propagation network with no BP step.

GRNN shows its superiority in terms of fitting capability and convergence speed and can converge to the global minimum compared with BPNN. Many missions in the remote sensing area, especially the remote sensing retrieval tasks, can be completed with the help of the GRNN model. Boyd et al. (2002) showed that GRNN has considerable potential for monitoring forest cover and its dynamics. Özerdem et al. (2017) estimated the soil moisture (SM) over agricultural areas with polarimetric decomposition models and a GRNN model. Şenkal (2010) developed a solar radiation estimation model in Turkey with GRNN and found a good agreement between the measured and predicted values based on the simulation. Although GRNN has achieved such remarkable success in the remote sensing area, the following drawback is also evident: GRNN would poorly perform when the training data is scarce; thus, sufficient training data must be collected to obtain a complete output distribution.

Although the above mentioned traditional NNs achieve great success in some area, they have somehow weak fitting ability due to their shallow structure. Deeper networks should be developed to address this problem. In the following, the introduced networks have a deeper layer than that of traditional NNs. These networks are called DL algorithms to distinguish them from traditional ML algorithms.

3.3. AE

AE is an important part of DL and can learn data coding in an unsupervised manner. AE can be divided into two parts: encoder and decoder (Fig. 4). Each part can be regarded as several hidden layers between an input layer and an output layer. The encoder reduces the dimension of the input high-dimensional sample data to output the low-dimensional encoded data. The low-dimensional encoded data are then taken as the decoder input. The output result, which has the same dimension as the input high-dimensional data of the encoder, is obtained through the dimension-raising operation of the decoder. BP algorithm is used to update the weight of the hidden layer to make the AE output as close as possible to the input. This condition is also used as a criterion to evaluate AE performance.

AE has been seldom applied in the field of remote sensing. However, some recent successful cases that adopt the AE model indicate its promising application prospect. Zhang et al. (2016a) introduced the AE model into the terrain classification of Polarimetric synthetic aperture radar (PolSAR) images and achieved remarkable improvement in classification accuracy. Liu and Wu (2016) adopted AE to identify geological disasters and found that AE outperforms the state-of-the-art classifiers in terms of efficiency and accuracy. Yuan and Jia (2015) proposed a water quality assessment method based on sparse AE and found that AE could achieve optimal recognition rates and is fit for future intelligent management. Overall, AE is suitable for compression and disentanglement tasks of high-dimensional data in the remote sensing area.

3.4. DBN

DBN, which is also another important part of DL, is a type of generative graphical model. Classic DBN contains several restricted Boltzmann machine (RBM) and ends with a BP layer (Fig. 5). Each RBM includes a visible layer, followed by a hidden layer. Each layer contains a certain number of neurons. Connections are found between RBMs but none between units within layers. Starting from the first layer, the upper hidden layer of the RBM serves as the next RBM visible layer input. During the training, the DBN is trained layer by layer, and the

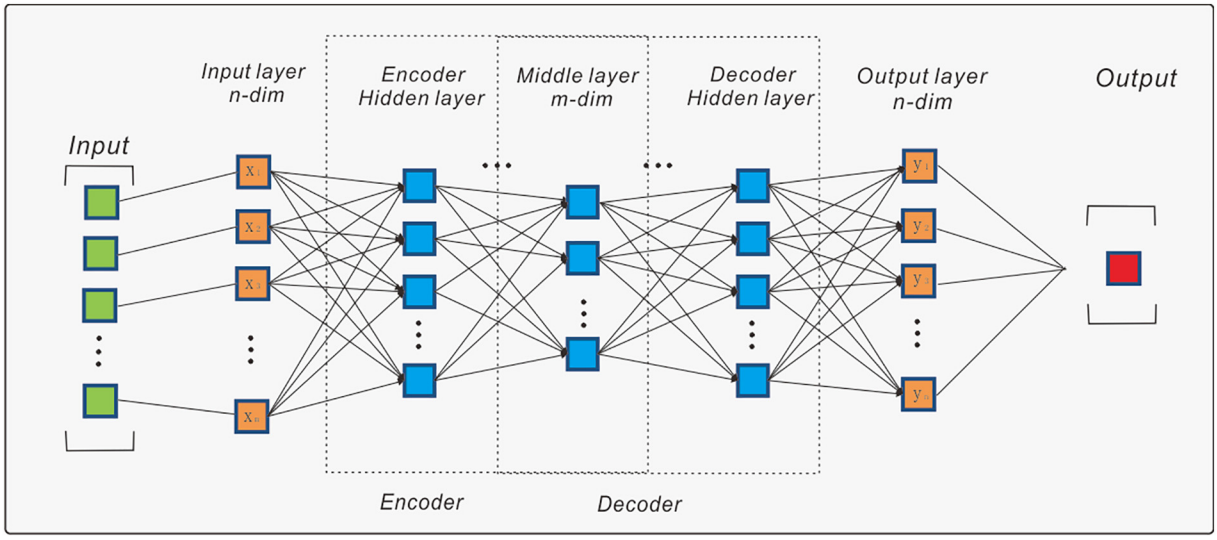

Fig. 4. AE structure.

weights of each layer are fixed layer by layer to obtain the approximate weight. Finally, the BP algorithm is used to fine-tune the weight of each layer and obtain the final DBN model.

Compared with some traditional NN models, such as BPNN, DBN overcomes the disadvantages of local optimum and long training time derived from the random initialization of weighted parameters. It only needs a local search for the parameter space; thus, the convergence time is considerably less. DBN could help solve many problems in remote sensing due to this meliorate. Shen et al. (2018b) directly estimated regional ground-level $PM_{2.5}$ (particulate matter with aerodynamic diameters < 2.5 μm) from satellite top-of-atmosphere (TOA) reflectance by DBN, providing an alternative technique to estimate the ground-level $PM_{2.5}$. Zhang et al. (2016a) and Zhong et al. (2017) introduced the DBN model to hyperspectral image classification work. They also provided better classification performance compared with traditional models, such as support vector machine (SVM), in most cases. Diao et al. (2016) adopted DBN to the object detection work and demonstrated the accuracy and efficiency of the DBN model.

3.5. CNN

CNN comprises a series of basic units stacked between the input and output layers (Fig. 6). Each basic unit may include the following operational layers: convolutional, pooling, and activation layers. In the convolution layer, several local filters are used to perform convolution operation on the input data. The output data with the same dimension as the input data are usually obtained. The pooling layer can obtain the low-dimensional data from the input data through various operations, such as max-pooling and average-pooling operations. The nonlinear operations in the activation layer increase the nonlinear fitting capability of CNN. The output and label data share the same dimension and should be as close as possible to each other through this series of shrink operations. CNN generally updates weight through BP in the same way as BPNN.

In the computer vision area, CNN shows its important and excellent function in the target recognition tasks and the remote sensing area. Lee and Kwon (2017) discussed the target recognition tasks with hyperspectral images. Jiang et al. (2018) extended the CNN application to recognize the target in SAR images. Both studies far exceeded the traditional recognition model. In addition, CNN can be applied to some retrieval tasks, such as SM retrieval (Wang et al., 2019a). Compared with the traditional NN, CNN abandons the fully connected layer and adopts a local connection. This approach reduces the computation and takes advantage of the relative position information in the sample. The shared convolution kernel is suitable for high-dimensional data processing. Nevertheless, CNN also has some disadvantages, such as the demand for massive training data and high computation cost.

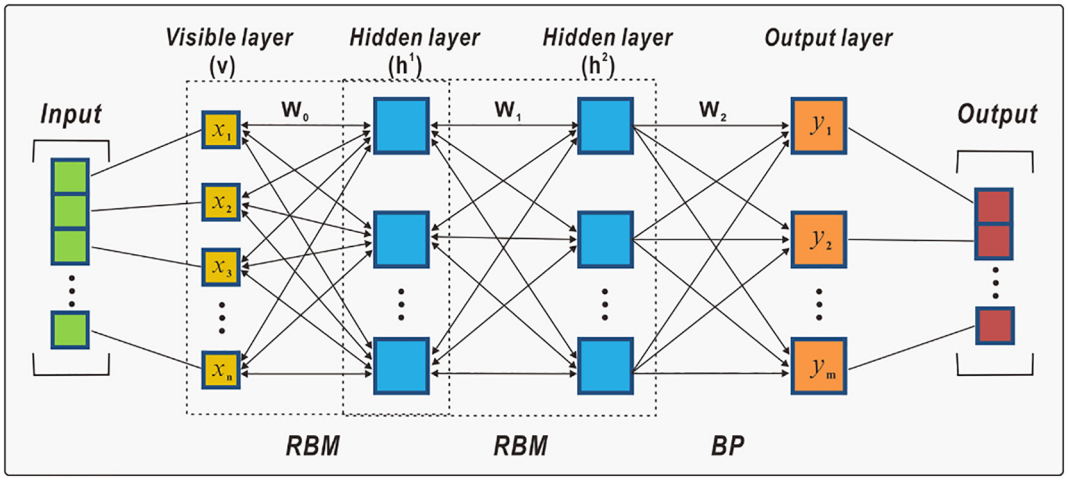

Fig. 5. DBN structure (Shen et al., 2018b).

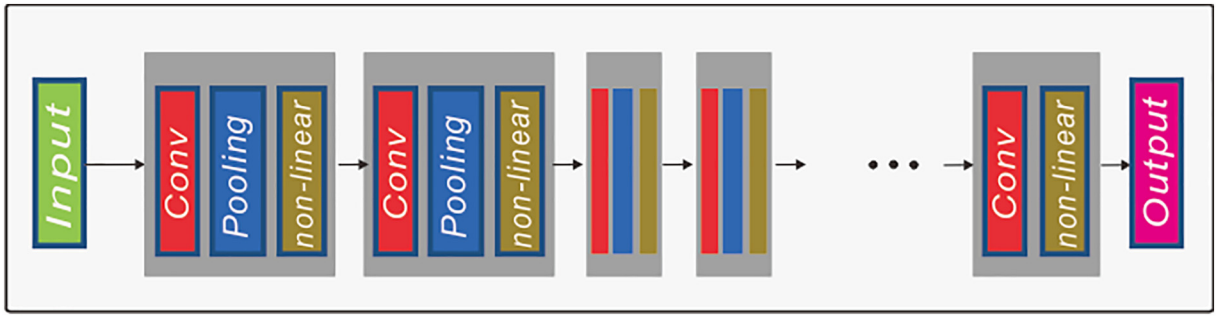

Fig. 6. CNN structure.

3.6. RNN, long short-term memory (LSTM) and gated recurrent unit (GRU)

A prerequisite of the model definition for an ordinary NN is the independence of the input/input, output/output, and input/output samples from each other. This condition makes it impossible to learn the relationship between samples. However, many samples are correlated in real datasets, such as sequential data, and the traditional network model cannot effectively cope with this correlation. RNN, LSTM and GRU are models that can deal with sequences, utilize the correlation between sequence data, and even generate sequences. As shown in Fig. 7(a), RNN has three main parts with several hidden layers. Each unit of the input sequence is successively inputted into RNN to obtain the corresponding output sequence unit of this phase and the information to transmit to the next phase. Such a task is performed to utilize the correlation within sequences. As an improved version of RNN, LSTM (Fig. 7(b)) contains forget, input, and output gates, which are used to control the filtering of the previous status. This structure aims to obtain previous statuses that are influential to the present instead of the most recent ones. Refer to Lipton et al. (2015) for the detailed algorithm and network structure of the above two models. As an excellent variant of LSTM, GRU (Fig. 7(c)) has far fewer parameters and simpler structure, whereas the same or even better effects compared with LSTM. GRU contains two main gates, namely, reset gate and update gate, to control the flow of long-term information. Reset gate controls how much previous information would be utilized in the current phase and update gate determines which parts of previous information would be abandoned in the current and next phases. The detailed algorithm of GRU can be found in Cho et al. (2014).

RNN has become an important model for analyzing time-series changes in remote sensing due to its excellent performance in short sequence processing. Besnard et al. (2017) established a model between forest disturbance and carbon balance in history with the RNN model. Freeman et al. (2018) applied the RNN model to predict air pollution time series with data from air monitoring stations in Kuwait. Ndikumana et al. (2018b) took advantage of RNN to deal with the agricultural classification study with multitemporal Sentinel-1 SAR data. RNN generally shows a remarkable advantage in dealing with short sequence problems. However, RNN would perform relatively poor in terms of long sequence data processing. As an evolution of RNN, LSTM can deal with the problems whose time sequence is long. You et al. (2017) proposed a model based on LSTM for crop field prediction, thereby allowing real-time forecasting. Yang et al. (2018) improved the prediction accuracy of sea surface temperature by combining spatial and temporal information with LSTM. Reddy and Prasad (2018)

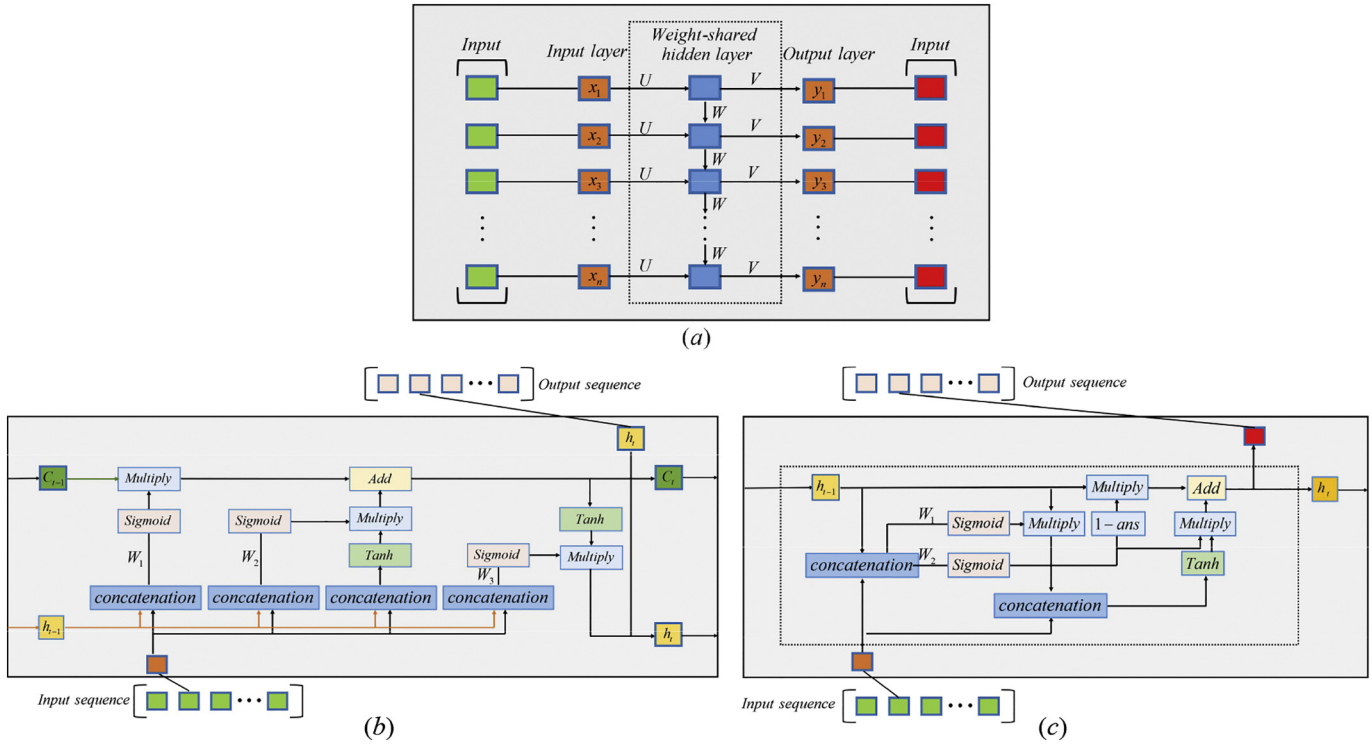

Fig. 7. Structures of (a) RNN, (b) LSTM and (c) GRU.

predicted the vegetation dynamics with far better performance by LSTM compared with the ordinary NN model. In addition, recent works (Fang et al., 2019; Fang et al., 2017) estimated the long-term SM by LSTM, which exhibits better generalization capability than that of traditional linear regression or autoregressive models. As a variant of LSTM, GRU can handle the long-term sequence with less training time but obtain results with even better quality. Ndikumana et al. (2018a) introduced GRU into the agriculture classification work with multi-temporal SAR data, which show some superiority over LSTM. Zhao et al. (2019) further compared the performance of RNN, LSTM and GRU in the early crop classification work with Sentinel-1A Imagery, in which GRU performs the best among the three algorithms.

4. Applications

4.1. Land cover

Land cover plays an important role in land planning and management as well as environmental analysis and applications. Land cover maps can be determined by classifying the different sources of remote sensing imagery, including optical and radar imagery (Augusteijn and Warrender, 1998; Benediktsson and Sveinsson, 1997; Lv et al., 2015; Shaker et al., 2019). Various land cover classification approaches using spectral and spatial information have been intensively studied (Blaschke, 2010; Duro et al., 2012; Foody, 1995; Hu et al., 2018a; Myint et al., 2011; Yan et al., 2006). These methods can interpret images by using the spectral features of each pixel and spatial features based on local regions or segmented objects. However, the performances of these methods are often affected by variations and noises within the class. The complex land structures or patterns are also difficult to discriminate by only using low-level spectral and spatial features. Therefore, considering the classification approaches using features at high levels is necessary.

DL has recently created huge breakthroughs in the remote sensing field, and these breakthroughs have been summarized in several review articles (John E. Ball et al., 2017; Ma et al., 2019; Zhang et al., 2016b; Zhu et al., 2017). Image classification is a common DL application. Accordingly, DL has been successfully applied to land cover classification and achieved impressive results (Zhang et al., 2018a; Zhao and Du, 2016; Zhao et al., 2015). Unlike traditional methods of using low-level spectral and spatial features for land cover classification, a notable advancement in the DL approach is its capability to learn discriminative features adaptively from images through supervised learning (Zeiler and Fergus, 2014). Noted that utilizing DL for land cover classification in remotely sensed images is similar to semantic segmentation in natural images, however, the latter usually segment natural images mainly based on spatial information, while the former further uses the rich spectral and temporal information in remotely sensed images to obtain better classification results. In addition, the inputs of the DL approach for land cover classification can be single source image data or a combination of multisource data, including optical, radar, and DEM data. The outputs are the scene-level category labels or pixel-level class map of the input image(s), in which a scene/pixel is categorized as a class label of maximal class probability. Accordingly, the DL approaches applied to the land cover classification in recent studies can be broadly divided into two categories according to spatial representation levels: scenes and pixels.

The scene-level approaches are often used to deal with land-use scene classification problems, which have been studied by Hu et al. (2015), Scott et al. (2017a), Wu et al. (2016), and Zhao et al. (2017). In this category of approaches, the input image is stepwise downsampled through the pooling layers in the model to support the extraction of multi-scale and multi-level features by convolutional layers, and then the fully connected layers are utilized for the final prediction of class probabilities. The present paper mainly reviewed the studies in terms of the pixel-level approaches, which are mostly used for pixel-to-pixel land cover classification, and classified each pixel in images by learning end-to-end deep models (Kussul et al., 2017; Li et al., 2016). This category of approaches usually labels each pixel/object of the input image based on the local window of the center pixel/object, more efficiently, pixel-to-pixel classification can be performed by fully convolutional networks. Specifically, in order to maintain the integrity of land structures and patterns in produced land cover maps, object-based image analysis (OBIA) (Zhang et al., 2018b), skeleton-based decomposition (Huang et al., 2018), and hierarchical segmentation (Tong et al., 2020) are combined with DL models to improve classification accuracy, separately, in which the input image is divided into more reasonable processing units or the classification results of DL are refined according to segmented units. Furthermore, Tracewski et al. (2017), Xing et al. (2018), and Xu et al. (2017) suggested that the auxiliary geotagged photographs benefit the land cover and use characterization and validation. Several well-known deep models are examined for complex land cover mapping (Mahdianpari et al., 2018). In several previous studies (Gaetano et al., 2018; Huang et al., 2018), a two-branch CNN architecture is designed to better cope with remote sensing imagery by separately dealing with panchromatic and multispectral information sources, and visible channels and multispectral channels in image, respectively. Recent studies (Ienco et al., 2019; Scott et al., 2018; Scott et al., 2017b) also investigated the fusion of multiple CNN classifiers into an aggregate classifier for land cover classification, which further enhances the classification ability of single classifier in a manner of multi-classifier ensemble. More recently, Interdonato et al. (2019) and Qiu et al. (2019) exploited the complementarity of convolutional and recurrent NN which capture different aspects of the data, and combined CNN and RNN into one end-to-end architecture to learn diverse spectral–spatial–temporal feature representation for accurate land cover classification.

Overall, DL approaches have been widely used in land cover classification and achieved advanced results. Combining CNNs with traditional image analysis techniques, such as OBIA and conditional random field (CRF), or integrated CNNs with other DL or ML classifiers, is conducive to improve the classification accuracy further. The combined use of multitemporal and multisource data also enhances the accuracy of land cover mapping. However, the manually labeled land cover dataset for the training of deep models is still inadequate for most tasks. This inadequacy limits the wide practical application of DL for land cover classification.

4.2. Vegetation parameters

Vegetation parameters, such as LAI, biomass, fractional vegetation cover (FVC), vegetation height, vegetation water content (VWC), and chlorophyll, can be retrieved from remote sensing data owing to the relationships between vegetation characteristics and remote sensing observations, such as backscattering, bright temperature, and various vegetation indexes calculated by combining visible and near-infrared bands. ANNs and DL succeeded in vegetation parameter retrieval and outperformed the traditional linear regression methods.

The sensitivity of different vegetation parameters to different remote sensing observations is distinct, and the auxiliary variables used for inversion are also diverse. Therefore, the selection of the most suitable auxiliary variables and models for inversion is an essential research topic. Frate and Solimini (2004) discussed the application of NN algorithms for retrieving forest biomass from multi-frequency (L- and P-bands) and multi-polarization (HH, VV, and HV) backscattering data. Li et al. (2010) developed a vegetation height inversion method based on BPNN to fit the relationship between the complex correction coefficients of polarimetric SAR interferometry and vegetation height. They also found that the inversion error caused by the ground interferometric estimation was reduced. Liu et al. (2002) presented the retrieval of wheat VWC from horizontally and vertically polarized brightness temperatures at L- and X-bands by an error propagation learning BPNN.

Various vegetation indexes, such as NDVI, enhanced vegetation index (EVI), and transformed chlorophyll absorption reflectance index together with diverse band reflections of Moderate-resolution Imaging Spectroradiometer (MODIS), Landsat Enhanced Thematic Mapper (ETM +), and Landsat 8, are used to retrieve vegetation biomass, chlorophyll, and LAI using ANN and radial basis function (RBF) (Liu et al., 2010; Liu et al., 2017; Xie et al., 2009; Yang et al., 2007; Yang et al., 2012). Moreover, Chen et al. (2015) used a nonlinear autoregressive network with exogenous input (NARX) model to learn the relationship between the input variables of four spectral bands and weight difference vegetation index and the output LAI. Accordingly, the feasibility of retrieving spatio-temporal LAI is demonstrated by a DL approach with field validation. Hosseini et al. (2019) used 14 polarimetric parameters from a time series of uninhabited aerial vehicle synthetic aperture radar airborne L-band data to estimate biomass for an intensively cropped site in western Canada. Their results show that NN provided more accurate estimates compared with those of multiple linear regression (MLR). Jin et al. (2019) estimated biomass based on 15 hyperspectral vegetation indexes by using the deep NN (DNN) algorithm. The three-band water index was the optimal vegetation index for biomass estimation. The results also show that the biomass estimation accuracy was further increased when LAI was combined with the 15 vegetation indexes.

NN and DL models usually require a large number of training samples. Some physical and empirical models can simulate canopy reflectivity, backscattering information, and vegetation parameter values, providing a considerable convenience for building datasets. Therefore, many studies concentrate on combining physical and statistical NN models to realize retrieval. Liao et al. (2013) retrieved wetland vegetation biomass based on NN combining the simulated data from the Michigan microwave canopy scattering model and the alternating polarization Envisat ASAR data. Trombetti et al. (2008) adopted ANN to retrieve VWC, linking radiative transfer model (RTM) and MODIS data. Yang et al. (2017) used simulations from the scattering by arbitrarily inclined leaves model and PROSPECT model to train BPNN-based FVC retrieval models. Fine spatial resolution FVC products were acquired by inputting Landsat 7 ETM+ and Landsat 8 OLI reflectance into the trained model. Jia et al. (2016) applied the same method to Chinese GF-1 wide-field view data and obtained high-quality FVC products. Wolanin et al. (2019) combined process-based modeling with the soil-canopy energy balance RTM (SCOPE) with Sentinel-2 and Landsat 8 optical remote sensing data and NN methods for crop estimation. The NN model can estimate GPP at the tested flux tower sites and outperform traditional empirical models.

A single remote sensing data source usually has temporal, spatial, and spectral resolution conflicts owing to the sensor characteristics. These conflicts result in limitations in the data application. The defects between the data can be remedied by fusing multisource remote sensing data. Many researchers also deal with this problem by using NN. An multilayer perceptron (MLP) model was used to integrate hyperspectral domain fusion and high spatial domain fusion techniques to deal with the non-linear canopy scattering between overstory and understory vegetation (Huang et al., 2011). Chai et al. (2012) proposed to train the NARX model for six typical vegetation types by fusing MODIS and SPOT time-series LAI to solve the discontinuity in time for single sensor-based LAI products. They also found that the predicted LAI of the NARX model is more continuous and accurate than the MODIS LAI. Xiao et al. (2014) trained a GRNN model over fused multitemporal data to estimate temporally continuous LAI. MODIS, CYCLOPES, and field-measured LAI, as well as MODIS reflectance products, were used to create the dataset. Similarly, Xiao et al. (2016) improved the model to produce a long time series Global Land Surface Satellite (GLASS) LAI product with an eight-day temporal resolution from Advanced Very High Resolution Radiometer (AVHRR) and MODIS reflectance data. The results indicated that the GLASS LAI values were closer to the high-resolution LAI maps than the MOD15 LAI values.

The NN, especially DL models, has advantages over the traditional linear regression methods in terms of retrieval accuracy of various vegetation parameters. However, the nondestructive acquisition of authentic in situ vegetation samples of the long time series is still a difficult problem in current studies. A new type of environmental remote sensing technique, namely, Global Navigation Satellite System Reflectometry (GNSS-R), provides a new mode for acquiring in situ vegetation parameters. Therefore, fusing the observations of multisource data, including optical, microwave, and GNSS-R, based on NN and DL, to retrieve vegetation parameters, is a valuable direction.

4.3. Agricultural yield prediction

Agricultural yield forecasts over large areas can help policymakers and grain marketing agencies plan for exports and imports (Chlingaryan et al., 2018; Johnson et al., 2016). Most of the current methods predict crop yield a few months before harvest by creating models between yields and influencing (such as weather, soil conditions, topography, disease, and vegetation growth conditions) and anthropogenic (such as irrigation and fertilizer management) factors. Some factors can be derived using remote sensing data over large areas. Desachy and Simpson (1994) developed a cerebellar model articulation controller NN. They found that the precision of the prediction model will be improved with the addition of remote sensing data (i.e., Landsat Thematic Mapper (TM) observation) based on agricultural data and meteorological variables. Moreover, NNs outperformed the traditional linear regression methods in the prediction of crop yield by using remote sensing vegetation indexes and other factors (Fortin et al., 2011; Kaul et al., 2005; Safa et al., 2014). Chlingaryan et al. (2018) reviewed the use of remote sensing data and the ML technique to estimate agricultural yields.

Spectral vegetation indexes related to agricultural yields are mathematical combinations of red, green, and infrared spectral bands based on the biophysiological relationships between crop characteristics and remote sensing features (Chlingaryan et al., 2018). The most frequently used index is NDVI. Li et al. (2007a) developed the shuffled complex evolution method developed at The University of Arizona (SCE-UA) optimization NN method to estimate corn and soybean yields using the historical yield data and MODIS and AVHRR NDVI. Fernandes et al. (2017) predicted sugarcane yields using MODIS NDVI and an ensemble model of NN. An NN wrapper with sequential backward elimination was applied to remove irrelevant and redundant features from the initial data set. Similar studies have also been conducted for other special vegetation indexes. Johnson et al. (2016) tested the MODIS NDVI, MODIS EVI, and AVHRR NDVI by creating Bayesian NNs in each hierarchically grouped region using crop yield data. They found that MODIS NDVI was an effective predictor for all three crops, and MODIS EVI served as an enhanced predictor. Panda et al. (2010) developed the BPNN model by using NDVI, green vegetation index, soil-adjusted vegetation index, and perpendicular vegetation indexes. The results indicated that the corn yield was accurately predicted using grid images of perpendicular vegetation index. Akhand et al. (2016) predicted the potato yield using AVHRR NDVI, vegetation health indices, vegetation condition index and temperature condition index. Kizil et al. (2012) explored the influence of irrigation on the lettuce yield by constructing an NN model using NDVI, simple ratio, chlorophyll green, and chlorophyll red edge. They found that a decrease in irrigation water led to a reduction in the lettuce yield.

Some other forms of NNs are also used to develop prediction models between auxiliary variables and crop yields. Savin et al. (2007) constructed a fuzzy NN (FNN) or granular NN (GNN) to predict crop yields by using Crop Growth Monitoring System simulation parameters and SPOT NDVI. Bose et al. (2016) applied the spiking NN (SNN) model to achieve a timely prediction of crop yields. The spatial accumulation of time series of MODIS NDVI and historical crop yield data were used to predict the crop yield with prolonged time. Although soil and climatic conditions play an important role in crop growth and yield, online

proximal soil sensing for the estimation of relevant soil properties remains a missing component in the management system. Pantazi et al. (2016) predicted wheat yield variation within the field based on multilayer soil data and remote sensing crop growth features. They also compared the following three NN models: counter propagation ANN, supervised Kohonen network (SKN), and XY-fusion network. Their results showed that SKN performed the best among the three models. Tiwari and Shukla (2019) used different geospatial features derived from NDVI, standard precipitation index, and vegetation condition index to predict the crop yield. A standard error BPNN was applied to construct the retrieval model to initiate learning from previous weather conditions.

DL includes representation learning, which extracts important features for object estimation from the input data. Kuwata and Shibasaki (2015) used a DL model of two inner product layers to simulate the relationship between meteorological parameters of MODIS EVI and crop yield. Their model can effectively predict crop yield and be further improved because the absolute spectral information is not exploited by the spectral vegetation indexes. You et al. (2017) used CNN and LSTM to discover relevant features from raw data automatically and then placed a Gaussian process layer on top of the neural architectures to account for spatial and temporal dependencies across data points explicitly. This approach outperformed competitive techniques in the predictive accuracy of county-level soybean yield prediction in the United States. Wang et al. (2018) later tested the transferability of the method proposed by You et al. (2017) to Argentina and Brazil. They found that the transfer learning approach achieved good results in the prediction of soybean yields in Brazil with a small amount of training data. A fast region-based CNN was chosen for the detection and counting of the number of flowers and mature and immature strawberries (Chen et al., 2019c). Kim et al. (2019) proposed the DNN model to develop the crop yield prediction model for the Midwestern US. This approach indicates that corn and soybean yield for a given year can be forecasted in advance.

With the addition of remote sensing data based on the meteorological data, the use of NN and DL to predict the crop yield is considerably improved compared with the traditional methods. At present, many types of retrieval models are available. However, the robustness of the prediction model is weak due to certain conditions, such as different crop types, terrain, and climate. Moreover, the predictions with high precision are usually limited merely in the study area. Therefore, improving the universality and migration of the crop yield prediction model is a popular but difficult point in future research.

4.4. Land surface and air temperature

LST and air temperature (Ta) are significant parameters that play crucial roles in related environmental studies and management activities, including surface energy fluxes, climate change, agricultural productivity, urban heat island monitoring, and industrial studies (Schoof and Pryor, 2001; Zhan et al., 2013). However, obtaining LST and Ta with both high spatial and temporal resolutions is usually difficult due to certain problems, such as limited measuring instruments, cloudy conditions, and sensor characteristics. Various NN and DL based methods have been developed for the estimation of LST and Ta in the last few years to overcome these issues. To date, numerous visible, near infrared and thermal infrared data, microwave measurements and satellite-derived products have been increasingly used in the LST and Ta field. With the application of different algorithms and data in previous literature, various LST and Ta products can be reconstructed with continuous high spatio-temporal resolutions.

LST retrieval has been widely discussed in previous literature. Aires et al. (2001) applied NNs to retrieve the surface skin temperature from the Special Sensor Microwave Imager observations. Venkateshwarlu et al. (2004) found a marked improvement in LST mapping by using ANN based on Landsat-5 TM thermal infrared data. Furthermore, the retrieval analyses have indicated that NN was a viable technique to resolve the typical ill-posed inversion problem by extracting potential information from training datasets (Mao et al., 2007; Mao et al., 2008a; Mao et al., 2008b). Also, Wang et al. (2013) established the MLP with two hidden layers to retrieve LST from hyperspectral thermal infrared data acquired by the Infrared atmospheric sounding interferometer instrument and achieved acceptable accuracy. Shwetha and Kumar (2016) demonstrated the applicability of combining infrared data and Microwave Polarization Difference Index derived from Advance Microwave Scanning Radiometer (AMSR)-Earth Observing System and AMSR2 sensors to predict LST with high spatio-temporal resolution under cloudy conditions based on the NN model. Especially, a deep dynamic learning NN coupled with five frequencies (10 channels, 10.7, 18.7, 23.8, 36.5, and 89 V/H GHz) acquired by AMSR2 data was utilized to retrieve the LST in a recent study (Mao et al., 2018). Recently, the CNN algorithm has been increasingly developed for LST retrieval. Tan et al. (2019) constructed CNN to retrieve LST from AMSR2 data in China. The stable and accurate result was achieved by using the combination of 12 V/H channels of 7.3, 10.65, 18.7, 23.8, 36.5, and 89 GHz. Furthermore, Wu et al. (2019) proposed a multiscale feature connected CNN model to reconstruct the LST of FengYun-2G and the Meteosat Second Generation-Spinning Enhanced Visible and Infrared Imager (MSG-SEVIRI) geostationary satellite datasets. In addition to the LST retrieval, some applications for LST downscaling and forecasting are presented. A genetic algorithm and self-organizing feature map NN was utilized to generate the high spatial-resolution LST at a subpixel scale by using the advanced spaceborne thermal emission and reflection radiometer (ASTER) visible, near infrared and thermal infrared data (Yang et al., 2010). Additionally, Goyal and Ojha (2012) also assessed the effectiveness of NNs to downscale LST. The NN-based model was statistically superior compared with the MLR-based model. Recently, a hybrid data-driven model using ensemble empirical mode composition coupled with a four-layer LSTM, is proposed by Zhang et al. (2018d) to forecast daily LST. The proposed model in their study significantly improved the prediction accuracy compared with that of the five other NNs.

In the Ta field, investigations are mainly focused on the forecasting and estimation of Ta. For the first type, Smith et al. (2006) once developed the Ward-style ANN architecture. They improved the Ta prediction by training multiple networks with different initial randomly-assigned weights. Other types of NNs such as BPNN, GRNN, and RBF method were employed and evaluated by Ustaoglu et al. (2008) for forecasting Ta time series. The results indicated that the three methods could provide reliable predictions. In contrast with the Ta forecast, satellite images were increasingly used for Ta estimation. Jang et al. (2004) employed a multilayer feed-forward NN (BPNN) to estimate Ta from AVHRR images. Satisfactory results were achieved when five bands of the AVHRR image, solar zenith angle, surface altitude and Julian day were used as input variables, along with 22 nodes selected in the hidden layer. In addition, an algorithm based on BPNN was also used for the retrieval of near-surface daily Ta from Landsat ETM+ images with reliable accuracy (Zhao et al., 2007). Subsequently, Mao et al. (2008b) developed an algorithm to estimate Ta based on ASTER data by synergizing a dynamic learning NN and the radiance transfer model. More particularly, the latest work of Shen et al. (2020) attempted to use the DL technique to estimate daily Ta across China by fusing remote sensing, station, simulation, and socioeconomic data. A 5-layer DBN was structured to establish the complex and non-linear physical relationships effectively, and significant improvements of the model accuracy could be obtained using such a technique compared with conventional models (Fig. 8).

Substantial progress in LST and Ta field has been observed in recent years. However, further studies are still necessary. With the rapid development of sensor techniques, the spatial and temporal resolutions of LST and Ta product must be improved in the future. Additionally, multi-source (i.e., reanalysis/forcing, vector, and dynamic POI data)

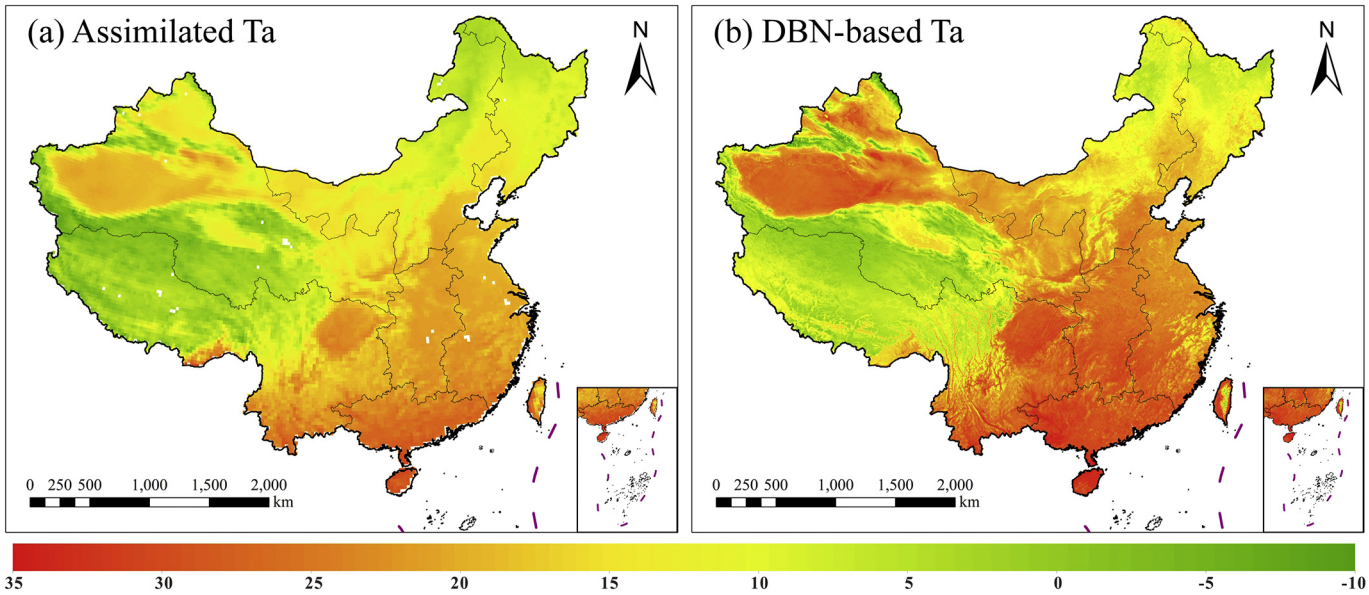

Fig. 8. Comparison of the annual daily maximum Ta map (unit: ˚C). (a) Assimilated Ta and (b) DBN-based Ta. The pixels in white indicate no data values (Shen et al., 2020).

data fusing is also facing considerable challenges. A few DL-based Ta studies are available, and algorithms, such as LSTM, should be utilized due to the considerable variations of Ta spatially and temporally. Lastly, the LST and Ta datasets should be applied in practical applications, such as climate conditions, urbanization development and ecosystem changes.

4.5. Aerosol

Aerosol is one of the most important atmospheric variables, and aerosol optical depth (AOD, or aerosol optical thickness), which is commonly monitored by satellite remote sensing, is usually retrieved through an atmospheric RTM (Levy et al., 2007). The mainstream retrieval methods for AOD include Dark Target and Deep Blue algorithms, which mainly utilize the information from red and blue bands. The AOD can also be estimated by statistical models with numerous observations of predictors and in-situ AOD due to the limitations of physical models in many assumptions regarding aerosols and surface properties (Nabavi et al., 2018). As previously mentioned, DL and NN have shown promising performance in inferring the statistical relationships. To our knowledge, the traditional NN has also been frequently used in the aerosol quantitative remote sensing problem. The input for NN-based aerosol remote sensing mainly includes the satellite radiance from multiple bands. Other auxiliary variables, such as angle information and topographical and meteorological conditions, are also occasionally included. The two main aspects of applications are as follows: i) AOD retrieval and ii) bias correction for AOD product.

Two different threads are present in the AOD retrieval problem. The first thread is to create a model between satellite radiance and AOD directly through NN models without considering the aerosol physical properties. The NN input is mainly satellite radiance, and auxiliary variables, such as solar viewing, cloud fraction, and land cover. Han et al. (2006) adopted a multilayer perceptron (MLP) network to retrieve AOD from multi-angular imaging spectroradiometric data. Vucetic et al. (2008) applied an ensemble of ten NN models to retrieve AOD with MODIS radiances for seven wavelengths between 0.47 and 2.1 μm, solar viewing, scattering angles, cloud-contamination indicators (MOD35), and surface type as inputs. Kolios and Hatzianastassiou (2019) also conducted a similar attempt by using Meteosat imagery, and brightness temperatures at the pixel level for the channels with spectral centers at 8.7, 10.8, and 12 μm were used. The retrieved results showed good consistency with the ground measured AOD. The above-mentioned results showed that NN-based AOD retrieval methods could serve as a useful complement to traditional retrieval methods. However, the physical properties of aerosols, which are vital for AOD, are ignored. Therefore, another thread is to create the NN model considering the aerosol physical properties. Taylor et al. (2014) introduced aerosol parameters, such as complex refractive indexes, single scattering albedo, and size distribution, into the NN model and found that model shows a good performance in the Saharan region. The aerosol type data can also be used to improve the NN retrieval (Patricia Castellanos and Silva, 2017).

In addition to the AOD retrieval problem, NN has also been widely applied in the bias correction problem. The main differences between NN-based AOD correction and retrieval are as follows: the former makes a bias correction with the NN input of the existing AOD product, whereas the latter estimates AOD by training a relationship between satellite radiance data and AOD. Satellite reflectance and angle information were used as the input variables for the NN-based AOD correction model. Lary et al. (2009) introduced the land cover information and the solar zenith, solar azimuth, and sensor zenith angles to correct the MODIS AOD product. The results showed that NN could largely improve the correlation with AEerosol RObotic NETwork (AERONET). Ristovski et al. (2012) also trained an NN-based estimator of retrieval uncertainty, and NN showed similar satisfactory performance. Some researchers later found that the bias between MODIS and AERONET AOD could be affected by numerous factors. Consequently, the input for the NN-based AOD correction model becomes complicated. Lanzaco et al. (2016) inputted modified day of the year (MDOY), MDOY direction, temperature, relative humidity, wind speed, and directions into a one-layer NN for MODIS AOD correction. The results showed that NN could be a valuable tool for enhancing MODIS AOD retrievals. The method was also adopted to obtain corrected AOD values taken from the MODIS AOD product (Lanzaco et al., 2017). Qin et al. (2018) recently utilized meteorological factors and cloud fraction for the correction of Modern-Era Retrospective analysis for Research and Applications Version 2 (MERRA-2) AOD with an optimized BPNN based on genetic algorithm. Accordingly, a largely improved product quality was achieved.

Although NN has been widely used in the aerosol retrieval and correction problem and achieved some satisfying results, DL has been hardly applied to this problem. DL has a stronger information

extraction capability and large potential to perform better on fitting the relationships between the multiband radiance information and AOD compared with NN. Therefore, exploring DL is a promising direction due to the success of NN in the above-mentioned AOD studies.

4.6. Particulate matter (PM)

PM is identified as a dust-related air pollutant that can increase morbidity and mortality risks. The satellite-derived AOD is the widely used parameter for ground-level PM retrieval from satellite remote sensing due to the inclusion of PM in the aerosol. Besides, the original satellite signals (i.e., red and blue channels of TOA reflectance and observation angles) for AOD retrieval were also adopted to estimate the ground PM concentrations. Statistical models have been popularly applied to infer ground PM from the satellite AOD or reflectance. In comparison with the parametric regression-based statistical models, NN and DL show advantages of fitting nonlinear relationships and involving fewer assumptions on the distribution of input and output variables. Therein, NN has achieved a relatively mature application in satellite-based PM estimation, and PM remote sensing with DL is now starting the stage with a rapid evolution. This review focuses on the NN and DL methods for PM remote sensing, and other methods can be found in a previous review (Chu et al., 2016).

Two main categories of NN have been introduced to estimate ground PM. The first category is the BPNN model. One of the earliest attempts to apply NN for remote sensing estimation of $PM_{2.5}$ was carried out by Gupta and Christopher (2009), which used the surface $PM_{2.5}$ data, satellite AOD product, and meteorological products in a BPNN model. Wu et al. (2012) later trained the BPNN model with Bayesian regularization for AOD-based $PM_{2.5}$ estimation, and a BPNN with convolutional layers was developed to consider spatiotemporal autocorrelation for the $PM_{2.5}$ estimation in the continental US (Di et al., 2016a). Moreover, a BPNN model (Wang et al., 2019b) for $PM_{2.5}$ estimation was recently trained with ground $PM_{2.5}$, satellite AOD observations, meteorological condition data, and emission data, which include auxiliary geographical parameters, such as land use, NDVI, elevation, and population density in China. The second category is a GRNN, which has also been applied for the estimation of ground $PM_{2.5}$ with the assistance of satellite AOD observations and meteorological variables in China (Li et al., 2017b). On this basis, a principal component analysis GRNN (PCA-GRNN) model was utilized to estimate ground-level PM_1 (aerodynamic diameters < 1 μm) concentrations from Himawari AOD observations in China (Zang et al., 2018; Zang et al., 2019).

DL has recently been employed to describe the complicated and nonlinear relationship between $PM_{2.5}$ and predictors effectively. Satellite-based DL models generally focus on the spatial estimation of $PM_{2.5}$. Li et al. (2017a) proposed a geo-intelligent DL approach for the estimation of $PM_{2.5}$ across China. Specifically, a DBN model was adopted with the input of satellite AOD, meteorological variables, and geographical correlation of $PM_{2.5}$. Fig. 9 shows the schematic of this model for $PM_{2.5}$ estimation, and DBN-based $PM_{2.5}$ estimates report a high consistency to ground station measurements (Fig. 10). Based on this model, an extended study was conducted to directly estimate $PM_{2.5}$ from satellite TOA reflectance (i.e., red, blue, and 2.1 μm channels of TOA reflectance) rather than satellite AOD (Shen et al., 2018b). The DL showed an excellent capacity to fit the complicated association among satellite reflectance, ground $PM_{2.5}$, and auxiliary factors. A recent work (Li et al., 2018a) developed an AE-based residual deep network, which was demonstrated by the $PM_{2.5}$ estimation using satellite AOD data in the Beijing–Tianjin–Tangshan area of China. Sun et al. (2019) proposed a DNN-based $PM_{2.5}$ prediction model based on Himawari AOD data and meteorological variables (denoted as PM25-DNN), and hourly $PM_{2.5}$ estimates were obtained in the Beijing–Tianjin–Hebei region of China. A newly published work (Park et al., 2020) applied a CNN model to estimate the daily $PM_{2.5}$ concentration of the conterminous US in 2011 by incorporating the AOD data, meteorological fields, and land-use data. On the other hand, Wen et al. (2019) developed a spatiotemporal convolutional LSTM extended model for the temporal prediction of $PM_{2.5}$. This model extracted spatiotemporal features by combining CNN and LSTM. The authors also incorporated satellite AOD data and meteorological variables to improve model prediction performance.

DL has attained early success for PM remote sensing in recent years, and this success may usher in rapid development in the near future. First, DL shows considerable potentials for the direct retrieval of PM from satellite TOA reflectance due to its remarkable capability for fitting nonlinear relationships and simulating physical models. The application of DL for direct PM retrieval in large geographical regions and on more satellite sensors deserves further attention. Second, the relationship between $PM_{2.5}$ and predictors is affected by a number of factors. Introducing earth “big data” (e.g., remote sensing, social sensing, and meteorological data) into PM remote sensing is a useful solution. In order to capture the nonlinear relationship from earth “big data”, DL is believed to be an effective tool. Therefore, PM remote sensing with the support of earth “big data” and DL is an important tendency.

4.7. Precipitation

Precipitation, a fundamental component of the global water cycle, is an essential parameter of meteorology, ecology, and hydrology. Remote sensing technology provides global-scale high-resolution satellite-based precipitation products to supplement the sparse and uneven networks of ground-based gauges and the absent validation of weather radar-rainfall. NNs have been successfully applied in satellite rainfall estimation (SRE). Multiple channels of geostationary orbit (GEO) satellite data, longwave infrared (IR), water vapor (WV) channels, and precipitation radar data are often incorporated for accurate precipitation retrieval. The NNs used in SRE have been classified into two categories: the first one relates to the different inverse problem approaches including physically-based methods and empirical or statistical methods; the second one relates to the different satellite inputs used to generate the rainfall estimates, including infrared imagery, passive microwave information and satellite fusion data (Tapiador et al., 2004). Compared with the classic approaches, NNs can maintain the quality of satellite measurements and improve the computational speed after training. Exploration of the underlying relationships between the geophysical parameters and precipitation is not required in the empirical approach for rainfall estimation using NNs. The University of Arizona established a system entitled Precipitation Estimation from Remotely Sensed Information using Artificial Neural Networks (PERSIANN) through a flexible three-layer feedforward NN model to estimate rainfall rates with IR satellite imagery and ground surface data (Hsu et al., 1997). The PERSIANN system considerably improved the SRE performance and could be updated using spatiotemporal limited observation gauge data simultaneously. A new SRE algorithm also based on NN called Precipitation Estimation from Remotely Sensed Information using Artificial Neural Networks Cloud Classification System (PERSIANN-CCS) was developed to improve the PERSIANN system due to its ability to extract cloud features (Hong et al., 2004). Bellerby et al. (2000) combined Tropical Rainfall Measuring Mission (TRMM) precipitation radar data and multispectral Geostationary Operational Environmental Satellite (GOES) imagery for NN training data to acquire high spatial and temporal resolution rain rates. The NN-based fusion results outperformed the optimized GOES Precipitation index (GPI) in the aspect of correlation with the gauge validation data.

DL techniques have been effectively used recently to improve the SRE accuracy and reduce the bias and false alarms. Tao et al. (2016b) used Stacked Denoising Auto-Encoders (SDAE) coupling with PERSIANN (referred to as PERSIANN-SDAE) to estimate large-scale precipitation from GEOS imageries. The performance of PERSIANN-SDAE showed the lowest averaged bias and Kullback-Leibler divergence

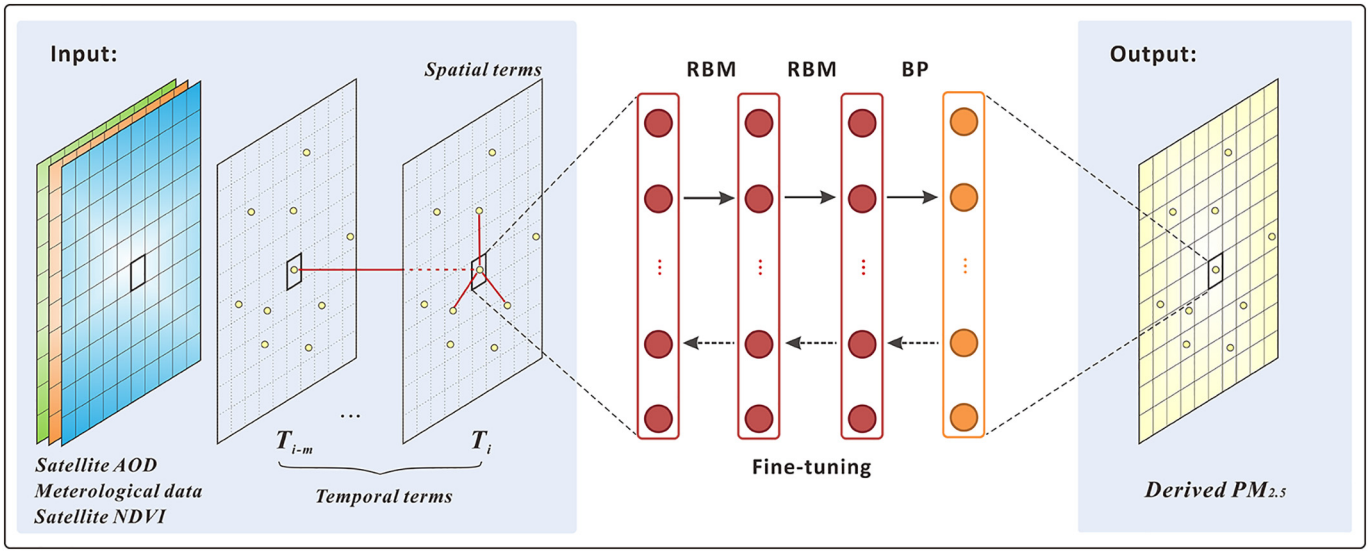

Fig. 9. Schematic of the geo-intelligent DBN model for $PM_{2.5}$ estimation. (Reprinted from Li et al. (2017a).)

compared with the three-layer NN model and PERSIANN-CCS model. This finding demonstrated that the PERSIANN-SDAE model could effectively capture the shape and the peak of the precipitation event with preserving the precipitation distribution. Tao et al. (2016a) also utilized the SDAE structured with a four-layer fully connected DNN to improve the quality of satellite precipitation products. The corrected results by SDAE model showed that the bias and false alarms were reduced. Furthermore, the SDAE was designed to identify useful features from bispectral satellite information to delineate precipitation regions, IR and WV channels included. The DL-IR method and the DL-IR + WV method based on SDAE model are superior to PERSIANN-CCS product with respect to the performances of rain/no-rain (R/NR) detection and the metric of critical success index (Tao et al., 2017; Tao et al., 2018). Real-valued precipitation estimation after R/NR classification based on SDAE model showed lower average bias, average mean squared error and higher correlation coefficient compared with those of the PERSIANN-CCS product (Tao et al., 2018). Sadeghi et al. (2019) proposed CNNs to estimate precipitation with the IR and WV channels and found that the proposed PERSIANN-CNN is more accurate than the PERSIANN-CCS and PERSIANN-SDAE models. Chen et al. (2019a) applied a non-parametric DNN approach in dual-polarization radar rainfall estimation to replace the physical model of the raindrop size distribution or the parametric model between the physical model and radar parameters. Their results showed the promising performance of this new method. Ayzel et al. (2019) used an all deep CNNs for radar-based precipitation nowcasting by utilizing a quality-controlled rainfall depth product composited from the 18 Doppler radars operated by the German Weather Service. Their results showed that parsimonious DL models could forecast a complex nature of a short-term precipitation field evolution and compete for the state-of-the-art performance with well-established nowcasting models based on optical flow techniques. Chen et al. (2019b) designed a two-stage DNN system to estimate rainfall using TRMM precipitation radar measurements, ground radar reflectivity, and gauge information. This DL method showed promising performance in regional and global rainfall mapping.

Therefore, DL techniques can achieve state-of-the-art performances in precipitation estimation. Furthermore, fusing multisource satellite-based precipitation products, radar data, and gauge station information to generate spatiotemporal continuous products on the global scale is a valuable yet challenging topic for studies.

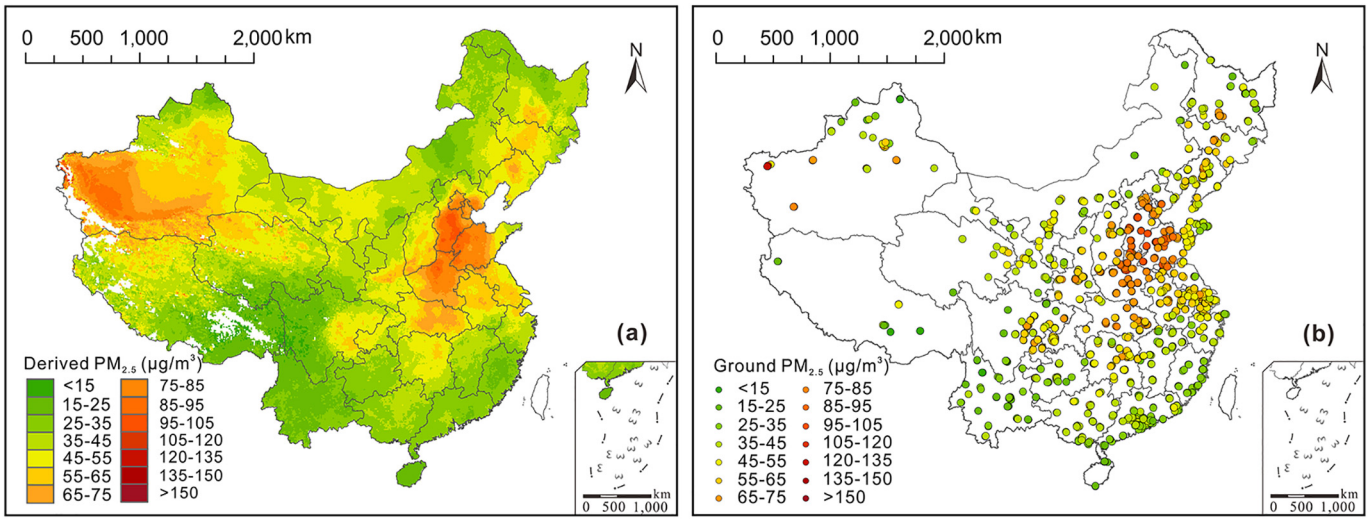

Fig. 10. Annual mean $PM_{2.5}$ distribution of China in 2015. (a) satellite-derived $PM_{2.5}$ and (b) ground-measured $PM_{2.5}$ in China. (Reprinted from Li et al. (2017a).)

4.8. Soil moisture (SM)

SM, especially surface (0–5 cm) SM, plays a vital part in the global water budget and water cycle. Accurate SM estimation is of utmost importance for many practical applications, such as flooding forecasting and drought monitoring.

SM retrieval is a complex process that depends on several interacting factors, such as soil texture, surface roughness, topography, and vegetation coverage. The lack of accurate understanding of the physical relationships between the terrestrial state and remote sensing observations and the unavailability of their associated parameters result in inaccurate SM estimation. Over the past two decades, NNs have been increasingly employed in the modeling of hydrological processes because of their capability in mapping the input–output relationship with limited understanding of the physical process. The NN relates SM to satellite observations (mainly C-/X-/L-band brightness temperatures for passive sensors and C-band backscattering coefficients for active instruments) and associated land surface properties, such as surface temperature and VWC. This condition allows for a simplification of the ill-posed inversion problems.

Scientific studies that investigate the use of ANNs for SM modeling and retrieval could be classified into three categories according to the types of used training data. First, ANNs could be trained with model-generated training data. A range of SM values is used to simulate brightness temperatures or backscattering coefficients based on radiative transfer or backscattering models. The former and the latter are taken as the output and input to ANNs, respectively. A substantial number of studies have implemented this approach to retrieve small-scale SM, which is further evaluated by experimental data from passive (Angiuli et al., 2008; Chai et al., 2009; Del Frate et al., 2003; Liou et al., 2001; Liu et al., 2002) or active (Baghdadi et al., 2002; Meng et al., 2018; Notarnicola et al., 2008; Paloscia et al., 2008; Paloscia et al., 2010; Pierdicca et al., 2008) microwave observations. Compared with other retrieval algorithms, such as the Bayesian method and the Nelder–Mead simplex algorithm, the effectiveness of ANN in terms of accuracy, stability, and speed for SM retrieval has been verified (Notarnicola et al., 2008; Paloscia et al., 2008; Pierdicca et al., 2008).

Second, the training of ANNs could be directly run with in-situ measurements. Rodríguez-Fernández et al. (2017a) and Gruber et al. (2014) attempted to retrieve continental and global SM from the Advanced SCATterometer (ASCAT) backscatter data and the Soil Moisture and Ocean Salinity (SMOS) brightness temperatures, respectively, using only in-situ SM data for ANN training. Santi et al. (2012) developed an ANN-based algorithm called “HydroAlgo” for hydrological purposes. HydroAlgo uses satellite-observed and simulated brightness temperatures and/or backscattering coefficients coupled with in-situ SM measurements to calibrate the ANNs. The model simulations are utilized to enrich the training datasets. This approach has been extensively used to investigate the potential of ANN in estimating regional SM from AMSR-E (Santi et al., 2016; Santi et al., 2012), Sentinel-1 SAR (Paloscia et al., 2013), and the Soil Moisture Active Passive (SMAP) observations (Santi et al., 2014). Merging of the different satellite observations to produce one single SM estimation is also tested on the basis of the HydroAlgo algorithm, including the fusion of SMAP and the AMSR2 observations (Santi et al., 2018a), and the combination of SMAP, AMSR2, and Sentinel-1 data (Santi et al., 2018b). Nevertheless, whether to train an ANN with in-situ data remains unclear due to the spatial scale mismatch between point-scale measurements (on the order of m^2) and large observed footprints by microwave remote sensing sensors (tens of km^2). Several strategies that can upscale in-situ SM observations to a coarse resolution have been developed to account for the aforementioned problem (Crow et al., 2012). However, performing global inversion using this approach is still difficult considering the sparse distribution of in-situ SM networks worldwide. Eroglu et al. (2019) first proved the potential of using ANNs to retrieve high spatio-temporal resolution from spaceborne GNSS reflections recorded by the Cyclone Global Navigation Satellite System (CYGNSS) mission. They used in-situ SM measurements from 18 International SM Network (ISMN) sites for ANN training, and encouraging results of CYGNSS-derived SM have been reported.

Finally, the use of global land surface model (LSM) simulations as the target data to train the ANNs has been increasingly applied for SM retrieval at large scales. Several studies have utilized this approach to develop global SM retrieval algorithms from either passive or active microwave sensors or a combination of the two. Aires et al. (2005), Kolassa et al. (2013), and Jiménez et al. (2013) realized a combined SM retrieval from passive microwave Special Sensor Microwave/Image (SSM/I) emissivities and active European Remote Sensing (ERS)-1 backscattering coefficients by using three different LSM-based SM reanalysis data. Rodriguez-Fernandez et al. (2015) and Kolassa et al. (2018) recently established the global SM retrieval from two SM-dedicated missions, namely, the SMOS and SMAP. The well-known European Center for Medium-range Weather Forecasts (ECMWF) and the Goddard Earth Observing System version 5 (GEOS-5) model are utilized as references to train the ANNs for SMOS and SMAP, respectively. Some studies also use ANNs to test the a priori merging of active and passive instruments, such as Advanced Scatterometer (ASCAT) and AMSR-E (Kolassa et al., 2016; Kolassa et al., 2017). Such a synergy strategy could provide considerably better results than a posteriori merging of SM products from each sensor. Compared with LSM simulations, several studies also utilize remotely sensed global SM products as a reference to train the ANNs. Accordingly, a consistent and long-term SM record at a global scale could be generated. Rodriguez-Fernandez et al. (2014) performed experiments using ANNs trained with two different reference SM products, namely, SMOS Level 3 SM and ECMWF model SM simulations. The SM retrievals based on the two inversion strategies were similar. Furthermore, Rodríguez-Fernández et al. (2016) used ANNs to extend the AMSR-E SM record in time by taking the global SMOS Level 3 SM dataset as the reference for training the algorithm. In another study, Rodríguez-Fernández et al. (2017b) utilized an SMOS Level-2 SM product to train an ANN and generated the new SMOS near-real-time SM product.

In addition to the SM retrieval, ANNs have also been exploited for downscaling information between sensors and SM reconstruction. Srivastava et al. (2013) first attempted to downscale the SMOS SM by applying the ANN to combine the SMOS SM and MODIS surface temperature at a local or regional scale. Alemohammad et al. (2018) then developed an ANN-based downscaling algorithm by disaggregating SMAP SM to 2.25 km spatial resolution. The downscaled SM shows better or equal accuracy compared with that of SMAP 9 km SM through ground validation. Cui et al. (2016) reconstructed Fengyun-3B SM across the Tibetan Plateau by using the ANN based on reconstructed MODIS products for the SM reconstruction (or infilling). Xing et al. (2017) proposed a novel SM image reconstruction algorithm by taking ANNs as a model to project complex and non-linear relationships between the in-situ measured and remotely sensed SM data.

From the above-mentioned discussion, the most widely used ANN structure is generally based on an MLP with two or more hidden layers, a non-linear activation function, and a BP learning rule. Some studies also focus on the use of GRNN. Özerdem et al. (2017) reported that a relationship between Radarsat-2 data and in situ SM over two agricultural sites was established by GRNN to estimate SM over agricultural areas. Xu et al. (2018a) utilized the GRNN to fuse the SMAP Level 3 passive SM product with in-situ SM measurements from five SM networks across the western continental US. Their results showed that this technique could improve the quality of SMAP retrieval. They also indicated that GRNN outperformed the MLR and traditional ANNs with the BP algorithm. Yuan et al. (2020) developed a point-surface collaborative inversion method for SM retrieval by using GRNN. Notably, the GRNN was trained on only “reliable” SM sites, which are determined through the application of the triple collocation method. The superiority of this approach over traditional RTMs and LSMs were

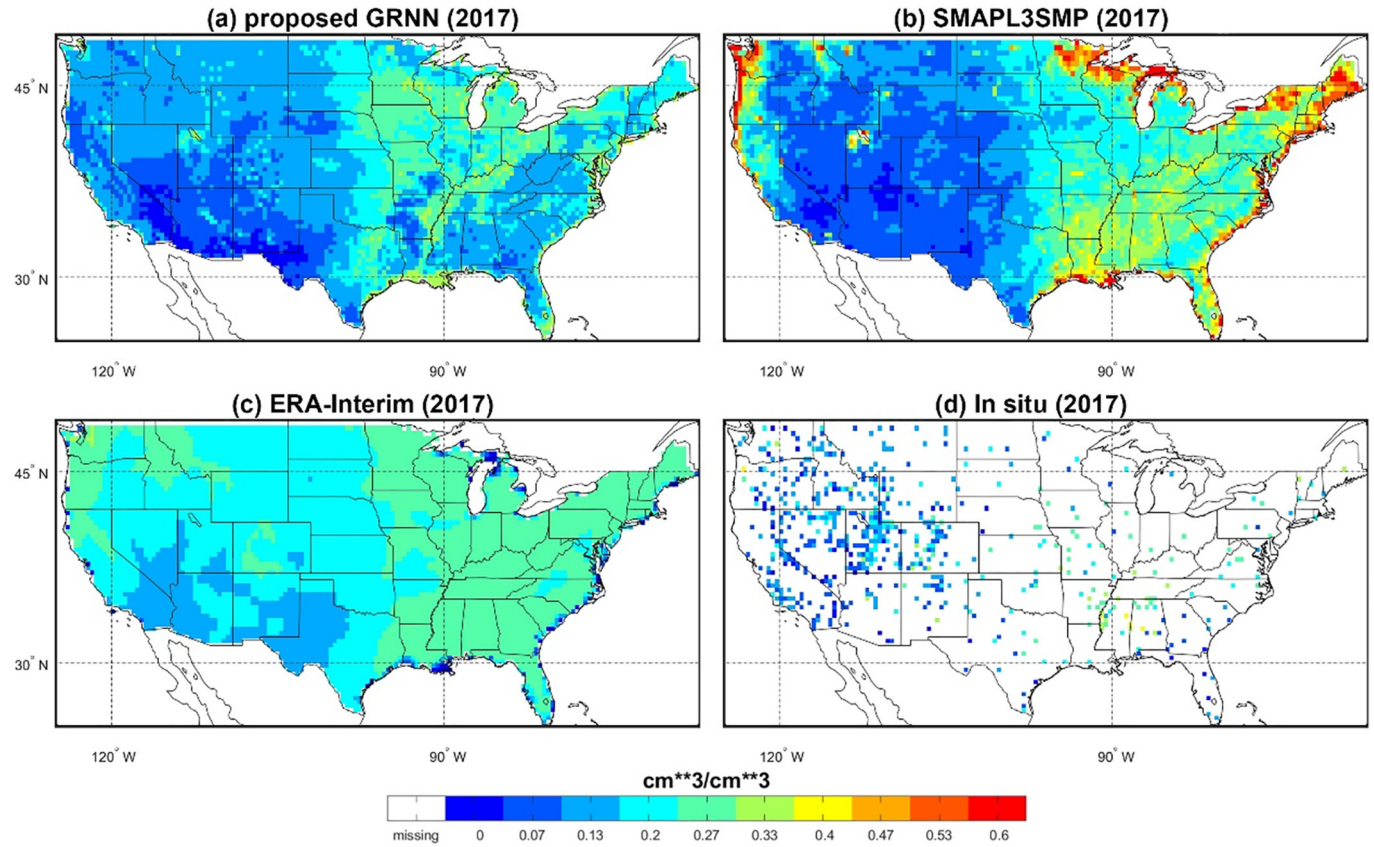

Fig. 11. Annual mean SSM map of the year 2017 for the following: (a) GRNN-based SSM retrieval, (b) official SMAP Level 3 radiometer SSM product (SPL3SMP), (c) ERA-Interim model simulations, and (d) in-situ measurements from ground SM networks across the continental US.
(Reprinted from https://doi.org/10.1016/j.jhydrol.2019.124351 (Yuan et al., 2020).)

demonstrated (Fig. 11). Several powerful DL techniques, such as DBN, deep feedforward NN (DFNN), LSTM, and CNN, have also been recently considered for SM modeling and retrieval. Song et al. (2016) used DBN to generate field-measured SM, with inputs of LST and LAI obtained from one experimental site. Fang et al. (2017) used LSTM to create a continental-scale seamless SM product that has high fidelity to SMAP with atmospheric forcing, model-simulated SM, and static physiographic attributes as inputs. The LSTM performance was further assessed in Fang et al. (2018). Zhang et al. (2017a) utilized DFNN to upscale in situ SM data for cropland in China by using the visible infrared imaging radiometer suite (VIIRS) raw data. In another study, a DFNN was used to estimate SM from AMSR2 data for the rapid, reliable, and spatially detailed drought monitoring in South Korea (Lee et al., 2018). Hu et al. (2018b) employed a CNN to AMSR-E brightness temperature images to retrieve the daily global SM. Similarly, Sobayo et al. (2018) developed a CNN-based regression model for estimating SM from the thermal infrared images of the farm area.

SM modeling and retrieval from different microwave sensors and across varied scales based on various ML/DL techniques have been effectively examined. However, DL techniques must account for the high heterogeneity of SM in space to accomplish an accurate SM estimation. Such techniques must also explore the comprehensive relationship between SM and all related parameters, such as albedo, soil texture, topography, surface roughness, and vegetation. Considering the model and observation errors, uncertainty assessment using DL-based retrieval algorithms needs further investigation.

4.9. Snow cover

Snow cover is an informative indicator of climate change because it can affect surface energy balance, hydrological processes, and ecosystem function (Xiao et al., 2018). On this basis, the accurate estimation of snow parameters, such as snow depth (SD), snow water equivalent (SWE), and fractional snow cover, is of considerable importance for research into climatology and hydrology. To date, ANNs have been widely applied in the estimation of SD, SWE, and fractional snow cover to improve the estimation accuracy of these snow parameters effectively.

The retrieval of SD (or SWE) is based on the nonlinear relationship constructed between passive microwave brightness temperature and SD (or SWE). Compared with the traditional linear models that inaccurately fit the nonlinear relationship, ANNs have been increasingly applied to estimate SD and SWE due to its good capability for nonlinear mapping. The input of ANN mainly includes vertically and horizontally polarized brightness temperature of 19 and 37 GHz and some auxiliary data, and the applications of ANN models have improved the estimation accuracy of SD and SWE. For example, ANNs have been utilized to retrieve SD (or SWE) with a spatial resolution of 25 km by fusing in-situ measurements and 19 and 37 GHz brightness temperatures from passive microwave sensors, including SSM/I and AMSR-E (Cao et al., 2008; Tedesco et al., 2004). In addition, ANNs have been trained with model simulations to retrieve SD (or SWE) (Davis et al., 1993; Tanikawa et al., 2015; Tedesco et al., 2004). Some studies have considered ancillary parameters, including physiographic and atmospheric data, as input parameters, together with brightness temperature, to train ANN-based retrieval models and correct the effects of terrain and forest cover on SD (or SWE) retrieval (Bair et al., 2018; Evora et al., 2008; Gan et al., 2009). The effectiveness of the ANN in retrieving SD (or SWE) compared with linear algorithms, such as Chang algorithm, has been validated in these studies. In addition to the retrieval of SD (or SWE), ANNs have been exploited for the fusion of several SWE products and SD reconstruction. Snauffer et al. (2018) applied ANN to improve SWE

products based on the fusion of six gridded SWE products. Li et al. (2019) applied ANN to map the change in SD on the present and the prior day and reconstruct the historical SD in the Tianshan Mountains of China based on the reanalysis of the temperature and precipitation datasets.

Fractional snow cover mapping can be generated by developing the relationship between fractional snow cover and satellite reflectance combined with auxiliary data, including normalized difference snow index (NDSI) constructed from MODIS bands 4 and 6 (or 7) and NDVI. Some studies have also applied ANNs to model the relationship between fractional snow cover and satellite reflectance effectively. For example, ANNs have been applied to estimate fractional snow cover using MODIS surface reflectance, NDSI, and NDVI as inputs, with reference fractional snow cover maps generated from high spatial resolution Landsat ETM + binary snow cover maps (Çiftçi et al., 2017; Dobreva and Klein, 2011). Their estimates compared favorably with those of the standard MODIS fractional snow cover product. In addition, ANN has been trained with samples simulated by a coupled atmosphere–surface RTM to estimate fractional snow cover (Gatebe et al., 2018). Some studies developed ANN models combined with MODIS and ancillary topographic data to estimate fractional snow cover in complex mountainous environments (Czyzowska-Wisniewski et al., 2015; Hou and Huang, 2014). DL models have shown their capability in automatic feature extraction and strong nonlinear expressiveness capability; however, these models have been applied in only a few snow studies. Nijhawan et al. (2018) proposed a multilayer DL framework approach to classify snow and non-snow for snow cover mapping by using diverse satellite imagery. Their proposed approach provided high classification accuracy, which outperformed ANN.

On this basis, ANNs have been widely applied to estimate snow parameters, including SD, SWE, and fractional snow cover. Thus, the capability of ANN to improve the estimation accuracy of snow parameters is demonstrated. DL models may be applied to improve the estimation accuracy of quantitative snow parameters further in the future, except for snow cover mapping. The combination of passive microwave data (or SD and SWE data) with low resolution and optical remote sensing data with high resolution based on ANN or DL models to downscale SD and SWE may be beneficial.

4.10. Evapotranspiration (ET_o)

Modeling of the reference ET_o process has remained to be a major priority of researchers because it plays a key role in the water cycle. At present, the FAO-Penman–Monteith (FAO-PM) method is recommended as an accepted standard technique for computing ET_o (Allen et al., 1998). However, a major limitation of this method is the requirement of various meteorological data, which are unavailable in many regions. The ET_o inversion is also a highly non-linear phenomenon because the ET_o process is regulated by numerous climatological factors. Thus, NNs have been increasingly employed in ET_o estimation to overcome these difficulties.

The capability of NNs to estimate small-scale ET_o has been tested by a multitude of studies. On the one hand, a combination of climatic variables, such as relative air humidity, air temperature, wind speed, solar radiation, and soil water content, can be treated as an input to NNs (Han and Felker, 1997; Kumar et al., 2008; Kumar et al., 2009; Kumar et al., 2002; Sudheer et al., 2003; Trajkovic et al., 2000; Trajkovic et al., 2003). On the other hand, numerous meteorological forcing can be reduced only on the basis of individual inputs, such as temperature data, because an explicit parameterization of physical relationships is unnecessary in NNs (Khoob, 2008a, 2008b; Rahimikhoob, 2010; Trajkovic, 2005). The superiority of NNs for estimating ET_o over traditional inversion approaches, including the FAO-PM method, the Hargreaves equation, multiple linear regression, and other empirical methods, has been demonstrated by these studies effectively.

Remote sensing techniques have recently provided an effective way for estimating ET_o on a large scale. This phenomenon is attributed to the terrestrial information from large extents related to ET_o obtained through remote sensing, such as NDVI, LST, surface net radiation, and land surface reflectance derived from MODIS. Therefore, the use of NNs and remotely sensed observations to facilitate the ET_o estimation has received considerable attention. Lu and Zhuang (2010) employed a BPNN to produce a daily ET_o product for the period of 2004–2005 by using remotely sensed observations from MODIS and meteorological data from 28 AmeriFlux sites in the conterminous US. Other studies also focus on the combination of AmeriFlux measurements and site-specific land surface products (NDVI and LST) derived from MODIS to train BPNNs for ET_o estimation (Chen et al., 2012; Panda et al., 2018; Wagle et al., 2017). A remote sensing-based BPNN model that aims to retrieve spatially distributed ET_o in Northwest China was recently established by linking the MODIS LST and reflectance data and site-specific ET_o calculated from meteorological data (Zhang et al., 2018e). The proposed approach could mitigate the dependence on meteorological data because they were required only in the training process and not in the application process. The comparison result between the BPNN and the well-known M5 model tree for estimating ET_o using MODIS products (Alipour et al., 2014) or modeling daily ET_o from National Oceanic and Atmospheric Administration (NOAA)/AVHRR satellite images (Rahimikhoob, 2016) showed that the correlation coefficients of the BPNN approach were slightly superior to the latter. In addition to the NN-based method, García-Pedrero et al. (2017) developed and evaluated a DL-based methodology that generated spatially distributed ET_o estimates by using CNN. The obtained results show that CNN models can estimate satisfactory ET_o maps.

However, the problem in estimating large-scale ET_o using ML/DL techniques is the scale mismatch issue, which results from the scale of in-situ measurements that does not match that of remote sensing satellites. Thus, many studies have discussed the possibility of using ML/DL-based approaches to upscale in-situ measured ET_o to the satellite footprint. Li et al. (2018c) conducted a comparison experiment by using six upscaling algorithms based on the AmeriFlux site measurements and remotely sensed data from MODIS in the Heihe River Basin. These algorithms include the area-weighted method, the integrated Priestley–Taylor equation, weighted area-to-area regression kriging (WATARK), BPNN, random forest (RF), and DBN. They found that the WATARK method efficiently performed over moderately heterogeneous areas. By contrast, the RF method efficiently performed over highly heterogeneous areas. Xu et al. (2018b) evaluated five ML algorithms, including BPNN, Cubist, DBN, RF, and SVM, for upscaling ET_o from point to regional scale. The ML methods are trained by relating daily ET_o derived from 36 AmeriFlux sites with remotely sensed variables and then applying it to the entire Heihe River Basin from 2012 to 2016. The results indicated that the five methods had nearly identical performances in estimating ET_o. However, the RF algorithm obtained slightly lower relative uncertainty than that of the four other ML algorithms.

Overall, although NNs have been extensively applied in ET_o modeling and retrieval, DL techniques are still at the initial stage of development for estimating ET_o but with substantial potential. Almost all the above-mentioned studies are also limited to the local or regional estimation of ET_o using ML/DL approaches. Future articles should focus on developing DL-based algorithms with global validity in ET_o modeling.

4.11. Radiation parameters

Radiation parameters are indispensable components for understanding the process of surface-atmosphere energy exchange and optimizing the sustainable energy utilization systems (Wang et al., 2012; Zhang et al., 2017b). The spatial distribution of radiation data is sparsely provided for most regions despite its importance. Over the past few years, many studies have been conducted to acquire accurate

surface and solar radiations. The NNs and DL methods along with satellite data have increasingly become popular in previous literature. One improvement is the capability of satellite data to provide continuous high-level retrieval products for reconstructing radiations over large areas. On the other side, NN and DL can better handle nonlinear and complex relationships than conventional methods (Kaba et al., 2018; Yadav and Chandel, 2014). For example, the visible, thermal, infrared channels and satellite-derived parameters obtained from Meteosat series of satellites, NOAA/AVHRR satellite, MODIS product and some geostationary satellites are widely used to estimate or forecast radiation parameters. This review mainly focused on summarizing the studies on solar and surface radiation.

For solar radiation estimation, researchers applied different NN architectures and satellite-derived data in previous literature. Şenkal and Kuleli (2009) once indicated that the use of NN with Meteosat-6 satellite data in the visible range is a cheap and effective way to estimate solar radiation over Turkey. Subsequently, Şenkal (2010) developed the GRNN and Şahin et al. (2013) investigated a multilayer feed-forward network to estimate solar radiation based on NOAA/AVHRR satellite-derived LST and achieved good results. In addition, the optimized NN ensemble model, which combines several NN models into an NN ensemble is also built in many studies. For instance, Eissa et al. (2013) once proposed an NN ensemble method to retrieve the direct normal, diffuse horizontal, and global horizontal irradiances by utilizing 6 thermal channels of the SEVIRI images. Linares-rodriguez et al. (2013) and Quesada-Ruiz et al. (2015) also exploited 11 channels of the Meteosat 9 satellite to estimate daily global solar radiation and hourly global horizontal irradiance, respectively. Notably, the optimized ANN ensemble models yielded reliable results even for overcast conditions. Compared to the NN, extreme learning machine (ELM), as a feed-forward NN, has been more successful in solar radiation estimation in other studies (Şahin, 2013; Şahin et al., 2014). In particular, DL was recently introduced for solar radiation estimation. In the work conducted by Kaba et al. (2018), a DL model was employed to estimate solar radiation for 34 stations in Turkey. The DL model applied in this study achieved comparable and precise results. Thus, DL can be a good alternative for similar studies. However, to obtain solar radiation for a large area, satellite data could be taken into consideration. Recently, Jiang et al. (2019) proposed a hybrid deep network named ResnetTL, which is mainly based on the CNN and MLP, to estimate hourly global solar radiation from the Multi-functional Transport Satellites (MTSAT). Notably, Yeom et al. (2019) used the complete L1b data set of Communication, Ocean, and Meteorological Satellite Meteorological Imager (MI) geostationary satellite, which comprised one visible and four infrared channels, to estimate solar radiation. In contrast with the above-mentioned studies, four data-driven models, namely, ANN, RF, SVR, and DNN were applied and compared with the physical model. The result expected the increasing utilization RF and DNN for solar radiation field estimation due to the accurate simulation of thin clouds. However, the physical model failed to achieve such a result.

In terms of solar radiation forecast field, a hybrid exponential smoothing state space model together with the BP MLP technique was applied for forecasting solar irradiance by using the geostationary satellite images; this approach showed superior accuracy than traditional forecasting models (Dong et al., 2014). According to Deo and Mehmet (2017), the feed-forward back-propagation (FFBP), as a popular ANN algorithm, was employed together with MODIS LST to forecast solar radiation. The result showed that FFBP outperformed MLR and auto-regressive integrated moving average algorithms.

In comparison with solar radiation, studies that use NN or DL along with satellite data to estimate surface radiations are relatively few. The existing literature could be classified into three main categories, which are upward, downward, and net radiation estimation. For instance, Wang et al. (2009) evaluated three methods to estimate instantaneous clear-sky surface upwelling longwave radiation (LWUP) with a high-resolution based on MODIS data. Smaller biases and root mean squared errors were found in the ANN model compared with the temperature-emissivity method and linear model. By contrast, Jiao et al. (2015) estimated the LWUP from TOA radiances of MODIS and VIIRS by using a hybrid method, which is the combination of extensive radiative transfer simulation and the ANN, and produced satisfactory retrieval results. Additionally, Nussbaumer and Pinker (2012) implemented a two-layer feed-forward NN to calculate the surface downwelling longwave radiation. Some studies subtracted upward fluxes from the dowelling fluxes to determine the net radiative fluxes. By contrast, Wang et al. (2012) directly estimated the surface longwave and shortwave net radiations by using a proposed typical feed-forward network, which was trained with a resilient BP algorithm.

Although several models have been proposed and efficiently performed for accurate radiation estimation and forecast, additional work is required in this field. Proper selection of the most relevant input variables with enhanced accuracy must be considered. Besides, increasing radiation estimation accuracy on different surfaces (i.e., tiled and tilted) should be further explored. Most existing studies focus on daily radiation and hourly radiation data. However, instantaneous radiation should also be given attention, especially for climate change and poor weather conditions.

4.12. Ocean color parameter

The essence of ocean color remote sensing is to retrieve the ocean color parameter content, which, in turn, is used to derive various biogeochemical constituents such as net primary production. Many ocean color sensors, such as Sea-viewing Wide Field-of-view Sensor (SeaWiFS), Medium Resolution Imaging Spectrometer (MERIS), ocean color monitor (OCM), and MODIS, with Hyperion images, have been used to retrieve some ocean color parameter products. Chlorophyll concentration is one of the most important ocean color data products, and its standard data products are derived using regression models (O'Reilly et al., 1998). The standard data products carry large uncertainties that are reduced by the NN. For example, Keiner (1999) derived oceanic chlorophyll a concentration by developing a simple three-layer NN algorithm with 10 nodes in the hidden layer using five SeaWiFS visible bands as inputs and found that the NN-based algorithm outperformed the cubic model and power polynomial models. Similarly, Musavi et al. (2002) constructed a feed-forward NN with an MLP network to estimate chlorophyll-a concentration from SeaWiFS data and the NN model outperformed the other empirical models. Corsini et al. (2003) compared RBF NN and MLP networks for chlorophyll concentration estimation in case II waters using MERIS data. The two NN algorithms outperformed the multi-linear regression model. The MLP-NN is a useful tool to estimate chlorophyll-a concentrations from MERIS and MODIS data in case II waters (Giménez et al., 2008). The coarse-resolution satellite images are unsuitable for chlorophyll-a estimation in the coastal water. Thus, Awad (2014) considered Earth Observing-1 satellite (EO-1) Hyperion images to estimate chlorophyll-a in the coastal zone based on supervised BPNN. The study proved the superiority of the BPNN to other regression models.

Physical or environmental parameters can improve the derivation of ocean color parameters using NN models. Tanaka et al. (2004) introduced an NN model by using Stuttgart Neural Network Simulator to estimate chlorophyll-a concentration, suspended matter and yellow substance from normalized water-leaving radiances (nLw) of the Ocean Color and Temperature Sensor data. Nagamani et al. (2007) estimated chlorophyll-a concentration using a 3-layer ANN trained with nLw from Ocean Colour Monitor satellite data. Nagamani et al. (2007) found that the ANN model is effective in modeling the non-linear relationship between nLw and chlorophyll-a concentration. Ferreira and Galo (2013) combined multispectral image and fluorometric measurements as ANN inputs to provide a good spatial inference result of chlorophyll-a concentration even in regions with small variations of chlorophyll-a concentration. Krasnopolsky et al. (2016) proposed an MLP model to fill

gaps in satellite data by relating the satellite-derived surface parameters (sea-surface temperature (SST), sea-surface height, and sea-surface salinity) to chlorophyll-a concentration to eliminate the systematic component and reduce the noise in satellite data. Jo et al. (2018) estimated chlorophyll-a concentration by using an NN algorithm trained with five microwave remote sensing measurements (SST, cloud, WV, precipitation, and winds) and geolocation data, offering a promising approach for filling gaps due to weather conditions.

DL techniques were gradually employed in the estimation of ocean color parameters. Cho et al. (2018) predicted four-day chlorophyll-a concentration by using a LSTM approach, which outperforms conventional NN methods. However, this study only used nine environmental variables from station measurements. Nock et al. (2019) developed a CNN architecture to parameterize the water column, including depth, bottom type, and inherent optical properties, from 89 spectral band hyperspectral imagery of water. The CNN performed better than RF and SVM methods. The retrieval of ocean color parameters using DL techniques is restricted due to the sparse and inadequate stations for measuring some parameters as sample data or validating the robustness and generalization capability of DL techniques. Additional efforts should be exerted to explore the potential of DL algorithms in ocean color remote sensing data.

5. Discussion and recommendations for future work

5.1. DL or physical models?

Environmental remote sensing involves many physical models that are grounded in systematic physical theories. In contrast with the physical models, DL has a long-standing problem of working as a black box. In other words, why and how the DL models work need further explanations. Consequently, the use of DL or physical models has triggered a wide debate in recent years. The issue of whether DL can replace the physical models bears the brunt. In the current stage, DL has been often used to supplement the physical models because it can effectively simulate the physical process and simplify the physical calculation for environmental remote sensing (Section 2.2). This has indicated some physical implications in the DL design. Therefore, we hold the belief that DL cannot completely replace the physical models, and the combination of physics-based models and DL may open a promising door for environmental remote sensing.

The synergy between physical models and DL deserves to be recommended for environmental remote sensing, which may be achieved by the following four main ways. **(1) Physical model simulation with DL**. Physical models generally take enormous computation in the forward simulation process for environmental modeling tasks. As an alternative, DL could be used for the forward simulation of physical models, in part or in whole, to save the computational cost. For example, an NN was trained by using simulated data from the radiance transfer model (i.e., MODerate resolution atmospheric TRANsmission version 4 (MODTRAN4)). The NN was then used for the LST retrieval based on satellite observations (Mao et al., 2007). In this process, the MODTRAN4 model is surrogated by an NN model. **(2) Physical model output calibration with DL**. Uncertainty often exists in the physical model parameters, thus resulting in errors in model outputs. With real observations and other auxiliary data, DL techniques could be adopted for the calibration of model outputs. Di et al. (2016b) utilized a BPNN model to calibrate GEOS-Chem outputs from 2001 to 2010 for the Northeastern US, in which ground monitoring data and other related predictors were used. Notably, the physical model outputs could also be used as input variables to aid DL modeling for the prediction of other parameters. For instance, Shen et al. (2020) indicated that the estimation of maximum air temperature could be improved by incorporating the Global Land Data Assimilation System simulations (e.g., SM content and albedo) into a DL architecture. **(3) Physics-guided DL architecture design**. With respecting the physical laws and mechanisms, certain DL architectures are designed for environmental remote sensing, which involves a deep combination of physics and DL. The DL architecture has a natural advantage to capture the potential physical relationship and of being interpretable. Schütt et al. (2017) proposed a molecular deep tensor NN, in which molecular properties are governed by the laws of quantum mechanics. **(4) Physics-constrained DL modeling**. The physical regularization constraints are designed in the loss function of DL models based on the physical mechanisms and knowledge to maintain the physical consistency in environmental modeling. The physically constrained cost function is then optimized to obtain a satisfying result that simultaneously has high model performance and physical consistency. For example, Karpatne et al. (2017) established a physics-constrained NN model for the problem of lake temperature modeling. The physics-based loss function was designed according to physical relationships among the temperature, density, and water depth. **Overall**, the combination of physical simulations and DL may not only boost the model accuracy but also improve the physical understanding in the environmental remote sensing.

5.2. Incorporating geographical laws into DL

Environmental phenomena occur in the realm of space and time, and they thus respect the geographical laws that describe the spatiotemporal autocorrelation and heterogeneity of environmental variables. The former suggests that the environmental variables are spatiotemporally correlated with themselves; the latter means that the relationship between environmental parameters varies in space and time. However, DL models are usually employed to establish global numeric relationships between variables without considering the geographical laws. The incorporation of geographical laws into DL enhances the exploration of environmental remote sensing studies.

First, the spatiotemporal autocorrelation of environmental variables is recommended to be introduced into DL models via the following two main ways. **(1) Introducing spatiotemporal autocorrelation as input variables into DL models**. The spatiotemporal autocorrelation of the environmental parameter could be captured as model-independent variables based on an inverse distance weighting or kernel-based weighting technique. They, along with other model predictors, are then inputted into the DL model for the environmental parameter prediction. For example, Li et al. (2017a) established a DBN model for the estimation of $PM_{2.5}$ by using satellite AOD, in which the spatiotemporal autocorrelations of $PM_{2.5}$ were used as two separate input variables captured by an inverse distance weighting strategy. However, only a shallow combination of spatiotemporal autocorrelation and DL is performed in the above process. **(2) Spatiotemporally constrained DL modeling**. The spatiotemporal structure of environmental variables may be included in the DL architecture or the dynamic learning of DL parameters to increase the interaction between spatiotemporal information and DL. Specifically, certain DL architectures could be designed to capture the spatiotemporal dependency of environmental parameters. For example, LSTM was designed to address the temporal dependency (Lipton et al., 2015); however, extending LSTM to the spatial context is difficult. In fact, the DL model design considering the spatiotemporal structure of environmental variables is highly challenging, and an alternative possible solution is to construct the constraint rules for spatiotemporal dependency in a DL model, like the above-mentioned physics-constrained DL modeling. Specifically, introducing a loss function with regularization constraints for spatiotemporal dependency may actually work for the combination of spatiotemporal autocorrelation and DL models.

Second, DL models considering spatiotemporal heterogeneity of environmental variables will also be of substantial interest to the remote sensing of the environment. Accordingly, geographically and temporally weighted DL (GTW-DL) models are believed to be a good choice. The DL models are separately established for individual locations and times to address the spatiotemporal heterogeneity, and these

DL models are then trained using spatiotemporally localized samples. Li et al. (2018b) recently proposed a geographically and temporally weighted GRNN model to cope with the spatiotemporal heterogeneity in the satellite-based $PM_{2.5}$ estimation. Two essential issues need to be addressed in the establishment of GTW-DL models. The first issue is the limited samples due to the difficulty in collecting sufficient samples in a spatiotemporally localized context. The other issue is computational cost, which is considerably enlarged for the establishment of spatiotemporally varying DL models. In short, the GTW-DL models hold remarkable potentials to cope with spatiotemporal heterogeneity, but they still need further explorations.

5.3. Small sample size and transfer learning

DL models often have a deep and complex structure and hence require a multitude of training data. However, the number of matchup samples in environmental remote sensing datasets is often limited. This limitation could be attributed to many aspects, such as missing satellite data due to cloud cover and sparse ground stations. This limitation of a small sample size could be improved to a certain degree by using transfer learning (Goodfellow et al., 2016). In this approach, parameters in a model pre-trained on large datasets can be fine-tuned with limited samples for optimal performance in the new task.

Specifically, the transfer learning applied in environmental remote sensing includes the following aspects. **(1) Region-based transfer learning**. The first approach first utilizes easily acquired geodata in a region to learn a robust deep model. The model is then extended to other regions to realize the transferring of the relation between environmental parameters and achieve high-precision environmental parameter retrieval results. An example of knowledge transfer from a city with sufficient samples to other similar cities with the small sample size problem has been presented in the study of Wei et al. (2016). **(2) Data-based transfer learning**. Data-based transfer learning is utilized to solve the problem of model generalization between multiple sensor images because the model trained on a sensor of images may not efficiently work when directly applied to other sensor images. Several land classification approaches (Huang et al., 2018; Tong et al., 2020) utilized such a technique to improve the performances of the model when applied to multi-sensor images.

The techniques and strategies in transfer learning, such as pre-training and fine-tuning, domain adaptation, are beneficial for solving small sample size problems in environmental remote sensing. The parameters in a model pre-trained on large datasets could be fine-tuned with limited samples to achieve optimal performance in the new task. Domain adaptation can also facilitate effective model performance trained on the source domain when applied to the target domain to accomplish a similar task. To date, although both approaches are helpful for promoting model performances, their acquired achievements are not that impressive as those of supervised learning.

6. Conclusion

A systematical review on the traditional NN and the most advanced DL methods in environmental remote sensing applications is presented in this paper. The DL techniques, which originated from ML fields, were initially used for image processing tasks. These techniques have been applied in remote sensing information classification and quantitative parameter retrieval in recent years, both from land cover mapping and environmental parameter retrieval. The investigation results showed that DL techniques have acquired tremendous achievements in environmental remote sensing. Finally, some new insights into the improvement of the DL tools for environmental remote sensing applications are also provided. For example, the combination of the physical and the DL models is a promising direction. Another potential research point is the incorporation of the geographical law into intelligent DL architecture. The traditional DL models are also largely dependent on many training samples. Combining transfer learning and DL may be a good choice to make these models effectively work in the limited sample condition.

CRediT authorship contribution statement

Qiangqiang Yuan:Conceptualization, Writing - original draft, Data curation, Writing - review & editing.**Huanfeng Shen**:Conceptualization, Data curation, Writing - original draft, Writing - review & editing.**Tongwen Li**:Investigation, Formal analysis, Writing - original draft, Data curation.**Zhiwei Li**:Investigation, Formal analysis, Writing - original draft, Data curation.**Shuwen Li**:Investigation, Formal analysis, Writing - original draft.**Yun Jiang**:Investigation, Formal analysis, Writing - original draft.**Hongzhang Xu**:Investigation, Formal analysis, Writing - original draft.**Weiwei Tan**:Investigation, Formal analysis, Writing - original draft.**Qianqian Yang**:Investigation, Formal analysis, Writing - original draft.**Jiwen Wang**:Investigation, Formal analysis, Writing - original draft.**Jianhao Gao**:Investigation, Formal analysis.**Liangpei Zhang**:Writing - review & editing.

Declaration of competing interest

The authors declare that they have no known competing financial interests or personal relationships that could have appeared to influence the work reported in this paper.

Acknowledgments

We gratefully acknowledge the support from the National Key Research and Development Program of China (Grant No. 2019YFB2102900), the Strategic Priority Research Program of the Chinese Academy of Sciences (Grant No. XDA19090104), and the National Natural Science Foundation of China (Grant Nos. 41922008 and 41820104006).

Appendix A. Nomenclature

AE	Autoencoder
AMSR2	Advanced microwave scanning radiometer 2
AOD	Aerosol optical depth
ASTER	Advanced Spaceborne Thermal Emission and Reflection Radiometer
AVHRR	Advanced Very High Resolution Radiometer
BNN	Bayesian neural networks
BPNN	Back-propagation neural network
CMAC	Cerebellar model articulation controller neural network
CNN	Convolutional neural network
CPANN	Counter propagation artificial neural network
DBN	Deep belief network
DFNN	Deep feedforward neural network
DL	Deep learning

DNN	Deep neural network
ECMWF	European Center for Medium-Range Weather Forecasts
EEMD	Ensemble empirical mode composition
ELM	Extreme learning machine
ET_o	Evapotranspiration
ETM +	Enhanced Thematic Mapper
FFBP	Feed-forward back-propagation
FNN	Fuzzy neural network
FVC	Fractional vegetation cover
GLASS	Global land surface satellite
GNN	Granular neural network
GOES	Geostationary operational environmental satellite
GRNN	Generalized regression neural network
GRU	Gated recurrent unit
LAI	Leaf area index
LSM	Land surface model
LST	Land surface temperature
LSTM	Long short-term memory
LWDN	Downwelling longwave radiation
LWUP	Upwelling longwave radiation
MCPN	Modified counter propagation network
MDOY	Modified day of year
MIMICS	Michigan microwave canopy scattering model
ML	Machine learning
MLP	Multilayer perceptron
MODIS	Moderate resolution imaging spectrometer
NARX	Nonlinear autoregressive networks with exogenous inputs
NDVI	Normalized difference vegetation index
nLw	Normalized water-leaving radiances
NN	Neural network
PM	Particulate matter
PVI	Perpendicular vegetation index
RBF	Radial basis function
RBM	Restricted Boltzmann machine
RF	Random forest
RNN	Recurrent neural network
RTM	Radiative transfer model
SD	Snow depth
SDAE	Stacked denoising auto-encoders
SeaWiFS	Sea-viewing wide field-of-view sensor
SKN	Supervised Kohonen network
SM	Soil moisture
SMAP	Soil moisture active passive
SMOS	Soil moisture and ocean salinity
SNN	Spiking neural networks
SNNS	Stuttgart neural network simulator
SRE	Satellite rainfall estimation
SVM	Support vector machine
SWE	Snow water equivalent
TM	Thematic Mapper
TOA	Top-of-atmosphere
TRMM	Tropical rainfall measuring mission
VWC	Vegetation water content
WATARK	Weighted area-to-area regression kriging
XYF	XY-fusion network

References

Aires, F., Prigent, C., Rothstein, M., 2001. A new neural network approach including first guess for retrieval of atmospheric water vapor, cloud liquid water path, surface temperature, and emissivities over land. J. Geophys. Res. 106, 14887–14907.

Aires, F., Prigent, C., Rossow, W., 2005. Sensitivity of satellite microwave and infrared observations to soil moisture at a global scale: 2. Global statistical relationships. J. Geophys. Res. Atmos. 110.

Akhand, K., Nizamuddin, M., Roytman, L., Kogan, F., 2016. Using remote sensing satellite data and artificial neural network for prediction of potato yield in Bangladesh. Proc. SPIE, Remote Sensing and Modeling of Ecosystems for Sustainability 9975, 997508.

Alemohammad, S.H., Kolassa, J., Prigent, C., Aires, F., Gentine, P., 2018. Global downscaling of remotely sensed soil moisture using neural networks. Hydrol. Earth Syst. Sci. 22, 5341–5356.

Alipour, A., Yarahmadi, J., Mahdavi, M., 2014. Comparative study of M5 model tree and artificial neural network in estimating reference evapotranspiration using MODIS products. J. Climatol. 2014, 1–11.

Allen, R.G., Pereira, L.S., Raes, D., Smith, M., 1998. Crop Evapotranspiration: Guidelines for Computing Crop Water Requirements. Food and Agriculture Organization, Rome, Italy (FAO Irrigation and Drainage Paper, No. 56. 300 p.).

Angiuli, E., Del Frate, F., Monerris, A., 2008. Application of neural networks to soil moisture retrievals from L-band radiometric data. In: Geoscience and Remote Sensing Symposium, 2008. IGARSS 2008. IEEE International (pp. II-61-II-64: IEEE).

Augusteijn, M.F., Warrender, C.E., 1998. Wetland classification using optical and radar data and neural network classification. Int. J. Remote Sens. 19, 1545–1560.

Awad, M., 2014. Sea water chlorophyll-a estimation using hyperspectral images and supervised artificial neural network. Ecological informatics 24, 60–68.

Ayzel, G., Heistermann, M., Sorokin, A., Nikitin, O., Lukyanova, O., 2019. All convolutional neural networks for radar-based precipitation nowcasting. Procedia Computer Science 150, 186–192.

Baghdadi, N., Gaultier, S., King, C., 2002. Retrieving surface roughness and soil moisture from synthetic aperture radar (SAR) data using neural networks. Can. J. Remote. Sens. 28, 701–711.

Bair, E.H., Abreu Calfa, A., Rittger, K., Dozier, J., 2018. Using machine learning for real-time estimates of snow water equivalent in the watersheds of Afghanistan. Cryosphere 12, 1579–1594.

Ball, J.E., Anderson, D.T., Chan, C.S., 2017. Comprehensive survey of deep learning in remote sensing: theories, tools, and challenges for the community. J. Appl. Remote. Sens. 11, 1.

Bellerby, T., Todd, M., Kniveton, D., Kidd, C., 2000. Rainfall estimation from a combination of TRMM precipitation radar and GOES multispectral satellite imagery through the use of an artificial neural network. J. Appl. Meteorol. 39, 2115–2128.

Benediktsson, J.A., Sveinsson, J.R., 1997. Feature extraction for multisource data classification with artificial neural networks. Int. J. Remote Sens. 18, 727–740.

Bengio, Y., Courville, A., Vincent, P., 2013. Representation learning: a review and new

perspectives. IEEE Trans. Pattern Anal. Mach. Intell. 35, 1798–1828.
Besnard, S., Carvalhais, N., Clevers, J., Dutrieux, L., Gans, F., Herold, M., Reichstein, M., Jung, M., 2017. Modelling effects of forest disturbance history on carbon balance: a deep learning approach using Landsat-time series. In: AGU Fall Meeting Abstracts.
Blaschke, T., 2010. Object based image analysis for remote sensing. ISPRS J. Photogramm. Remote Sens. 65, 2–16.
Bose, P., Kasabov, N.K., Bruzzone, L., Hartono, R.N., 2016. Spiking neural networks for crop yield estimation based on spatiotemporal analysis of image time series. IEEE Trans. Geosci. Remote Sens. 54 (11).
Boyd, D.S., Foody, G.M., Ripple, W.J., 2002. Evaluation of approaches for forest cover estimation in the Pacific Northwest, USA, using remote sensing. Appl. Geogr. 22, 375–392.
Cao, Y., Yang, X., Zhu, X., 2008. Retrieval snow depth by artificial neural network methodology from integrated AMSR-E and in-situ data—a case study in Qinghai-Tibet Plateau. Chin. Geogr. Sci. 18, 356–360.
Castellanos, P., Silva, A., 2017. The GEOS-5 neural network retrieval (NNR) for AOD. In: AGU Fall Meeting.
Chai, S.-S., Walker, J.P., Makarynskyy, O., Kuhn, M., Veenendaal, B., West, G., 2009. Use of soil moisture variability in artificial neural network retrieval of soil moisture. Remote Sens. 2, 166–190.
Chai, L., Qu, Y., Zhang, L., Liang, S., Wang, J., 2012. Estimating time-series leaf area index based on recurrent nonlinear autoregressive neural networks with exogenous inputs. Int. J. Remote Sens. 33, 5712–5731.
Chen, Z., Shi, R., Zhang, S., 2012. An artificial neural network approach to estimate evapotranspiration from remote sensing and AmeriFlux data. Front. Earth Sci. 7, 103–111.
Chen, B., Wu, Z., Wang, J., Dong, J., Guan, L., Chen, J., Yang, K., Xie, G., 2015. Spatio-temporal prediction of leaf area index of rubber plantation using HJ-1A/1B CCD images and recurrent neural network. ISPRS J. Photogramm. Remote Sens. 102, 148–160.
Chen, H., Chandrasekar, V., Cifelli, R., 2019a. A Deep Learning Approach to Dual-Polarization Radar Rainfall Estimation. IEEE, pp. 1–2.
Chen, H., Chandrasekar, V., Tan, H., Cifelli, R., 2019b. Rainfall estimation from ground radar and TRMM precipitation radar using hybrid deep neural networks. Geophys. Res. Lett. 46, 10669–10678.
Chen, Y., Lee, W.S., Gan, H., Peres, N., Fraisse, C., Zhang, Y., He, Y., 2019c. Strawberry yield prediction based on a deep neural network using high-resolution aerial orthoimages. Remote Sens. 11.
Cheng, Q., Shen, H., Zhang, L., Yuan, Q., Zeng, C., 2014. Cloud removal for remotely sensed images by similar pixel replacement guided with a spatio-temporal MRF model. ISPRS J. Photogramm. Remote Sens. 92, 54–68.
Chlingaryan, A., Sukkarieh, S., Whelan, B., 2018. Machine learning approaches for crop yield prediction and nitrogen status estimation in precision agriculture: a review. Comput. Electron. Agric. 151, 61–69.
Cho, K., van Merrienboer, B., Gulcehre, C., Bahdanau, D., Bougares, F., Schwenk, H., Bengio, Y., 2014. Learning Phrase Representations Using RNN Encoder-Decoder for Statistical Machine Translation. (In, arXiv e-prints).
Cho, H., Choi, U., Park, H., 2018. Deep learning application to time-series prediction of daily chlorophyll-a concentration. WIT Trans. Ecol. Environ. 215, 157–163.
Chu, Y., Liu, Y., Li, X., Liu, Z., Lu, H., Lu, Y., Mao, Z., Chen, X., Li, N., Ren, M., 2016. A review on predicting ground PM2.5 concentration using satellite aerosol optical depth. Atmosphere 7, 129.
Çiftçi, B., Kuter, S., Akyürek, Z., Weber, G., 2017. Fractional snow cover mapping by artificial neural networks and support vector machines. ISPRS Annals of the Photogrammetry, Remote Sensing Spatial Information Sciences 4, 179.
Corsini, G., Diani, M., Grasso, R., De Martino, M., Mantero, P., Serpico, S.B., 2003. Radial basis function and multilayer perceptron neural networks for sea water optically active parameter estimation in case II waters: a comparison. Int. J. Remote Sens. 24, 3917–3931.
Crow, W.T., Berg, A.A., Cosh, M.H., Loew, A., Mohanty, B.P., Panciera, R., de Rosnay, P., Ryu, D., Walker, J.P., 2012. Upscaling sparse ground-based soil moisture observations for the validation of coarse-resolution satellite soil moisture products. Rev. Geophys. 50.
Cui, Y., Long, D., Hong, Y., Zeng, C., Zhou, J., Han, Z., Liu, R., Wan, W., 2016. Validation and reconstruction of FY-3B/MWRI soil moisture using an artificial neural network based on reconstructed MODIS optical products over the Tibetan Plateau. J. Hydrol. 543, 242–254.
Czyzowska-Wisniewski, E.H., van Leeuwen, W.J., Hirschboeck, K.K., Marsh, S.E., Wisniewski, W.T., 2015. Fractional snow cover estimation in complex alpine-forested environments using an artificial neural network. Remote Sens. Environ. 156, 403–417.
Das, M., Ghosh, S.K., 2017. A deep-learning-based forecasting ensemble to predict missing data for remote sensing analysis. IEEE Journal of Selected Topics in Applied Earth Observations and Remote Sensing 10, 5228–5236.
Davis, D.T., Chen, Z., Tsang, L., Hwang, J.-N., Chang, A.T., 1993. Retrieval of snow parameters by iterative inversion of a neural network. IEEE Trans. Geosci. Remote Sens. 31, 842–852.
Del Frate, F., Ferrazzoli, P., Schiavon, G., 2003. Retrieving soil moisture and agricultural variables by microwave radiometry using neural networks. Remote Sens. Environ. 84, 174–183.
Deo, R.C., Mehmet, Ş., 2017. Forecasting long-term global solar radiation with an ANN algorithm coupled with satellite-derived (MODIS) land surface temperature (LST) for regional locations in Queensland. Renew. Sust. Energ. Rev. 72, 828–848.
Desachy, J., Simpson, G., 1994. Crop yield prediction using a CMAC neural network. In: Proc. SPIE Image and Signal Processing for Remote Sensing. 2315. pp. 160–171.
Di Noia, A., Hasekamp, O.P., 2018. Neural networks and support vector machines and their application to aerosol and cloud remote sensing: a review. In: Springer Series in Light Scattering. Springer, pp. 279–329.
Di, Q., Kloog, I., Koutrakis, P., Lyapustin, A., Wang, Y., Schwartz, J., 2016a. Assessing PM2.5 exposures with high spatiotemporal resolution across the continental United States. Environ. Sci. Technol. 50, 4712–4721.
Di, Q., Koutrakis, P., Schwartz, J., 2016b. A hybrid prediction model for PM2.5 mass and components using a chemical transport model and land use regression. Atmos. Environ. 131, 390–399.
Diao, W., Sun, X., Zheng, X., Dou, F., Wang, H., Fu, K., 2016. Efficient saliency-based object detection in remote sensing images using deep belief networks. IEEE Geosci. Remote Sens. Lett. 13, 137–141.
Dobreva, I.D., Klein, A.G., 2011. Fractional snow cover mapping through artificial neural network analysis of MODIS surface reflectance. Remote Sens. Environ. 115, 3355–3366.
Dong, Z., Yang, D., Reindl, T., Walsh, W.M., 2014. Satellite image analysis and a hybrid ESSS/ANN model to forecast solar irradiance in the tropics. Energy Convers. Manag. 79, 66–73.
Duro, D.C., Franklin, S.E., Dubé, M.G., 2012. A comparison of pixel-based and object-based image analysis with selected machine learning algorithms for the classification of agricultural landscapes using SPOT-5 HRG imagery. Remote Sens. Environ. 118, 259–272.
Eissa, Y., Marpu, P.R., Gherboudj, I., Ghedira, H., Ouarda, T.B.M.J., Chiesa, M., 2013. Artificial neural network based model for retrieval of the direct normal, diffuse horizontal and global horizontal irradiances using SEVIRI images. Sol. Energy 89, 1–16.
Eroglu, O., Kurum, M., Boyd, D., Gurbuz, A.C., 2019. High spatio-temporal resolution CYGNSS soil moisture estimates using artificial neural networks. Remote Sens. 11, 2272.
Evora, N.D., Tapsoba, D., De Seve, D., 2008. Combining artificial neural network models, geostatistics, and passive microwave data for snow water equivalent retrieval and mapping. IEEE Transactions on Geoscience Remote Sensing 46, 1925–1939.
Fang, K., Shen, C., Kifer, D., Yang, X., 2017. Prolongation of SMAP to spatiotemporally seamless coverage of continental U.S. using a deep learning neural network. Geophys. Res. Lett. 44, 11,030–11,039.
Fang, K., Pan, M., Shen, C., 2018. The value of SMAP for long-term soil moisture estimation with the help of deep learning. IEEE Trans. Geosci. Remote Sens. 1–13.
Fang, K., Pan, M., Shen, C., 2019. The value of SMAP for long-term soil moisture estimation with the help of deep learning. IEEE Trans. Geosci. Remote Sens. 57, 2221–2233.
Fernandes, J.L., Ebecken, N.F.F., Esquerdo, J.C.D.M., 2017. Sugarcane yield prediction in Brazil using NDVI time series and neural networks ensemble. Int. J. Remote Sens. 38, 4631–4644.
Ferreira, M.S., Galo, M.B.T., 2013. Chlorophyll a spatial inference using artificial neural network from multispectral images and in situ measurements. An. Acad. Bras. Cienc. 85, 519–532.
Foody, G.M., 1995. Land cover classification by an artificial neural network with ancillary information. Int. J. Geogr. Inf. Syst. 9, 527–542.
Fortin, J.G., Anctil, F., Parent, L.-É., Bolinder, M.A., 2011. Site-specific early season potato yield forecast by neural network in Eastern Canada. Precis. Agric. 12, 905–923.
Frate, F.D., Solimini, D., 2004. On neural network algorithms for retrieving forest biomass from SAR data. IEEE Trans. Geosci. Remote Sens. 42, 11.
Freeman, B.S., Taylor, G., Gharabaghi, B., The, J., 2018. Forecasting air quality time series using deep learning. J. Air Waste Manage. Assoc. 68, 866–886.
Gaetano, R., Ienco, D., Ose, K., Cresson, R., 2018. A two-branch CNN architecture for land cover classification of PAN and MS imagery. Remote Sens. 10, 1746.
Gan, T.Y., Kalinga, O., Singh, P., 2009. Comparison of snow water equivalent retrieved from SSM/I passive microwave data using artificial neural network, projection pursuit and nonlinear regressions. Remote Sens. Environ. 113, 919–927.
García-Pedrero, A.M., Gonzalo-Martín, C., Lillo-Saavedra, M.F., Rodriguéz-Esparragón, D., Menasalvas, E., 2017. Convolutional neural networks for estimating spatially distributed evapotranspiration. In: Image and Signal Processing for Remote Sensing XXIII. International Society for Optics and Photonics, pp. 104270P.
Gatebe, C., Li, W., Chen, N., Fan, Y., Poudyal, R., Brucker, L., Stamnes, K., 2018. Snow-covered area using machine learning techniques. In: IGARSS 2018-2018 IEEE International Geoscience and Remote Sensing Symposium. IEEE, pp. 6291–6293.
Giménez, Á.M., Estévez, M.D., Vilas, L.G., Palenzuela, J.M.T., 2008. Development of a Neural Network to Retrieve Chlorophyll Concentrations from MERIS Images in the Galician Coastal Waters.
Goodfellow, I., Bengio, Y., Courville, A., 2016. Deep Learning. MIT press.
Goyal, M.K., Ojha, C.S.P., 2012. Downscaling of surface temperature for lake catchment in an arid region in India using linear multiple regression and neural networks. Int. J. Climatol. 32, 552–566.
Gruber, A., Paloscia, S., Santi, E., Notarnicola, C., Pasolli, L., Smolander, T., Pulliainen, J., Mittelbach, H., Dorigo, W., Wagner, W., 2014. Performance inter-comparison of soil moisture retrieval models for the MetOp-A ASCAT instrument. In: Geoscience and Remote Sensing Symposium (IGARSS), 2014 IEEE International. IEEE, pp. 2455–2458.
Gupta, P., Christopher, S.A., 2009. Particulate matter air quality assessment using integrated surface, satellite, and meteorological products: 2. A neural network approach. J. Geophys. Res. Atmos. 114, D20205.
Han, H., Felker, P., 1997. Estimation of daily soil water evaporation using an artificial neural network. J. Arid Environ. 37, 251–260.
Han, B., Vucetic, S., Braverman, A., Obradovic, Z., 2006. A statistical complement to deterministic algorithms for the retrieval of aerosol optical thickness from radiance data. Eng. Appl. Artif. Intell. 19, 787–795.
Hong, Y., Hsu, K.-L., Sorooshian, S., Gao, X., 2004. Precipitation estimation from remotely

sensed imagery using an artificial neural network cloud classification system. J. Appl. Meteorol. 43, 1834–1853.
Hosseini, M., McNairn, H., Mitchell, S., Robertson, L.D., Davidson, A., Homayouni, S., 2019. Synthetic aperture radar and optical satellite data for estimating the biomass of corn. Int. J. Appl. Earth Obs. Geoinf. 83.
Hou, J., Huang, C., 2014. Improving mountainous snow cover fraction mapping via artificial neural networks combined with MODIS and ancillary topographic data. IEEE Transactions on Geoscience Remote Sensing 52, 5601–5611.
Hsu, K., Gao, X., Sorooshian, S., Gupta, H.V., 1997. Precipitation estimation from remotely sensed information using artificial neural networks. J. Appl. Meteorol. 36, 1176–1190.
Hu, F., Xia, G.-S., Hu, J., Zhang, L., 2015. Transferring deep convolutional neural networks for the scene classification of high-resolution remote sensing imagery. Remote Sens. 7, 14680–14707.
Hu, T., Huang, X., Li, J., Zhang, L., 2018a. A novel co-training approach for urban land cover mapping with unclear Landsat time series imagery. Remote Sens. Environ. 217, 144–157.
Hu, Z., Xu, L., Yu, B., 2018b. Soil moisture retrieval using convolutional neural networks: application to passive microwave remote sensing. ISPRS - International Archives of the Photogrammetry, Remote Sensing and Spatial Information Sciences XLII-3, 583–586.
Huang, J., Zeng, Y., Wu, W., Mao, K., Xu, J., Su, W., 2011. Estimation of overstory and understory leaf area index by combining hyperion and panchromatic QuickBird data using neural network method. Sens. Lett. 9, 964–973.
Huang, B., Zhao, B., Song, Y., 2018. Urban land-use mapping using a deep convolutional neural network with high spatial resolution multispectral remote sensing imagery. Remote Sens. Environ. 214, 73–86.
Ienco, D., Interdonato, R., Gaetano, R., Minh, D.H.T., 2019. Combining Sentinel-1 and Sentinel-2 satellite image time series for land cover mapping via a multi-source deep learning architecture. ISPRS J. Photogramm. Remote Sens. 158, 11–22.
Interdonato, R., Ienco, D., Gaetano, R., Ose, K., 2019. DuPLO: a DUal view Point deep Learning architecture for time series classificatiOn. ISPRS J. Photogramm. Remote Sens. 149, 91–104.
Jang, J.-D., Viau, A.A., Anctil, F., 2004. Neural network estimation of air temperatures from AVHRR data. Int. J. Remote Sens. 25, 4541–4554.
Jia, K., Liang, S., Gu, X., Baret, F., Wei, X., Wang, X., Yao, Y., Yang, L., Li, Y., 2016. Fractional vegetation cover estimation algorithm for Chinese GF-1 wide field view data. Remote Sens. Environ. 177, 184–191.
Jiang, T., Cui, Z.Y., Zhou, Z., Cao, Z.J., Ieee, 2018. Data augmentation with Gabor filter in deep convolutional neural networks for Sar target recognition. In: IGARSS 2018–2018 IEEE International Geoscience and Remote Sensing Symposium. Ieee, New York, pp. 689–692.
Jiang, H., Lu, N., Qin, J., Tang, W., Yao, L., 2019. A deep learning algorithm to estimate hourly global solar radiation from geostationary satellite data. Renew. Sust. Energ. Rev. 114, 109327.
Jiao, Z., Yan, G., Zhao, J., Wang, T., Chen, L., 2015. Estimation of surface upward longwave radiation from MODIS and VIIRS clear-sky data in the Tibetan Plateau. Remote Sens. Environ. 162, 221–237.
Jiménez, C., Clark, D.B., Kolassa, J., Aires, F., Prigent, C., 2013. A joint analysis of modeled soil moisture fields and satellite observations. J. Geophys. Res. Atmos. 118, 6771–6782.
Jin, X., Li, Z., Feng, H., Renc, Z., Li, S., 2019. Deep neural network algorithm for estimating maize biomass based on simulated Sentinel 2A vegetation indices and leaf area index. The Crop Journal 8, 87–97.
Jo, Y.-H., Kim, D.-W., Kim, H., 2018. Chlorophyll concentration derived from microwave remote sensing measurements using artificial neural network algorithm. Journal of Marine Science and Technology-Taiwan 26, 102–110.
Johnson, M.D., Hsieh, W.W., Cannon, A.J., Davidson, A., Bédard, F., 2016. Crop yield forecasting on the Canadian prairies by remotely sensed vegetation indices and machine learning methods. Agric. For. Meteorol. 218–219, 74–84.
Kaba, K., Sarıgül, M., Avcı, M., Kandırmaz, H.M., 2018. Estimation of daily global solar radiation using deep learning model. Energy 162, 126–135.
Karpatne, A., Watkins, W., Read, J., Kumar, V., 2017. Physics-guided Neural Networks (PGNN): An Application in Lake Temperature Modeling. (arXiv preprint arXiv:1710.11431).
Kaul, M., Hill, R.L., Walthall, C., 2005. Artificial neural networks for corn and soybean yield prediction. Agric. Syst. 85, 1–18.
Keiner, L.E., 1999. Estimating oceanic chlorophyll concentrations with neural networks. Int. J. Remote Sens. 20, 189–194.
Khoob, A.R., 2008a. Artificial neural network estimation of reference evapotranspiration from pan evaporation in a semi-arid environment. Irrig. Sci. 27, 35–39.
Khoob, A.R., 2008b. Comparative study of Hargreaves's and artificial neural network's methodologies in estimating reference evapotranspiration in a semiarid environment. Irrig. Sci. 26, 253–259.
Kim, N., Ha, K.-J., Park, N.-W., Cho, J., Hong, S., Lee, Y.-W., 2019. A comparison between major artificial intelligence models for crop yield prediction: case study of the midwestern United States, 2006–2015. International Journal of Geo-information 8.
Kizil, Ü., Genç, L., Inalpulat, M., Şapolyo, D., Mirik, M., 2012. Lettuce (Lactuca sativa L.) yield prediction under water stress using artificial neural network (ANN) model and vegetation indices. Zemdirbyste 99, 10.
Kolassa, J., Aires, F., Polcher, J., Prigent, C., Jimenez, C., Pereira, J.-M., 2013. Soil moisture retrieval from multi-instrument observations: information content analysis and retrieval methodology. J. Geophys. Res. Atmos. 118, 4847–4859.
Kolassa, J., Gentine, P., Prigent, C., Aires, F., 2016. Soil moisture retrieval from AMSR-E and ASCAT microwave observation synergy. Part 1: satellite data analysis. Remote Sens. Environ. 173, 1–14.
Kolassa, J., Reichle, R.H., Draper, C.S., 2017. Merging active and passive microwave observations in soil moisture data assimilation. Remote Sens. Environ. 191, 117–130.
Kolassa, J., Reichle, R.H., Liu, Q., Alemohammad, S.H., Gentine, P., Aida, K., Asanuma, J., Bircher, S., Caldwell, T., Colliander, A., Cosh, M., Collins, C.H., Jackson, T.J., Martinez-Fernandez, J., McNairn, H., Pacheco, A., Thibeault, M., Walker, J.P., 2018. Estimating surface soil moisture from SMAP observations using a neural network technique. Remote Sens. Environ. 204, 43–59.
Kolios, S., Hatzianastassiou, N., 2019. Quantitative aerosol optical depth detection during dust outbreaks from Meteosat imagery using an artificial neural network model. Remote Sens. 11, 1022.
Krasnopolsky, V., Nadiga, S., Mehra, A., Bayler, E., Behringer, D., 2016. Neural networks technique for filling gaps in satellite measurements: application to ocean color observations. Computational intelligence and neuroscience 2016, 29.
Kumar, M., Raghuwanshi, N., Singh, R., Wallender, W., Pruitt, W., 2002. Estimating evapotranspiration using artificial neural network. J. Irrig. Drain. Eng. 128, 224–233.
Kumar, M., Bandyopadhyay, A., Raghuwanshi, N.S., Singh, R., 2008. Comparative study of conventional and artificial neural network-based ETo estimation models. Irrig. Sci. 26, 531.
Kumar, M., Raghuwanshi, N., Singh, R., 2009. Development and validation of GANN model for evapotranspiration estimation. J. Hydrol. Eng. 14, 131–140.
Kussul, N., Lavreniuk, M., Skakun, S., Shelestov, A., 2017. Deep learning classification of land cover and crop types using remote sensing data. IEEE Geosci. Remote Sens. Lett. 14, 778–782.
Kuwata, K., Shibasaki, R., 2015. Estimating crop yields with deep learning and remotely sensed data. In: Geoscience & Remote Sensing Symposium. IEEE.
Lanzaco, B.L., Olcese, L.E., Palancar, G.G., Toselli, B.M., 2016. A method to improve MODIS AOD values: application to South America. Aerosol Air Qual. Res. 16, 1509–1522.
Lanzaco, B.L., Olcese, L.E., Palancar, G.G., Toselli, B.M., 2017. An improved aerosol optical depth map based on machine-learning and MODIS data: development and application in South America. Aerosol Air Qual. Res. 17, 1623–1636.
Lary, D., Remer, L., MacNeill, D., Roscoe, B., Paradise, S., 2009. Machine learning and Bias correction of MODIS aerosol optical depth. IEEE Geosci. Remote Sens. Lett. 6, 694–698.
LeCun, Y., Bengio, Y., Hinton, G., 2015. Deep learning. Nature 521, 436.
Lee, H., Kwon, H., 2017. Going deeper with contextual CNN for hyperspectral image classification. IEEE Trans. Image Process. 26, 4843–4855.
Lee, C.s., Sohn, E., Park, J.D., Jang, J.-D., 2018. Estimation of soil moisture using deep learning based on satellite data: a case study of South Korea. GIScience & Remote Sensing 56, 43–67.
Levy, R.C., Remer, L.A., Mattoo, S., Vermote, E.F., Kaufman, Y.J., 2007. Second-generation operational algorithm: retrieval of aerosol properties over land from inversion of moderate resolution imaging spectroradiometer spectral reflectance. J. Geophys. Res. Atmos. 112 (n/a-n/a).
Li, A., Liang, S., Wang, A., Qin, J., 2007a. Estimating crop yield from multi-temporal satellite data using multivariate regression and neural network techniques. Photogramm. Eng. Remote Sens. 79, 9.
Li, G., Song, K., Niu, S., 2007b. Soybean LAI estimation with in-situ collected hyperspectral data based on BP-neural networks. In: 2007 3rd International Conference on Recent Advances in Space Technologies, pp. 331–336.
Li, T., Liang, D., Huang, H., Zhu, J., 2010. A new method based on the BP neural network to improve the accuracy of inversion of the vegetation height. In: 2010 International Conference on Image Analysis and Signal Processing. IEEE, pp. 544–547.
Li, W.J., Fu, H.H., Yu, L., Gong, P., Feng, D.L., Li, C.C., Clinton, N., 2016. Stacked autoencoder-based deep learning for remote-sensing image classification: a case study of African land-cover mapping. Int. J. Remote Sens. 37, 5632–5646.
Li, T., Shen, H., Yuan, Q., Zhang, X., Zhang, L., 2017a. Estimating ground-level PM2.5 by fusing satellite and station observations: a geo-intelligent deep learning approach. Geophys. Res. Lett. 44, 11,985–911,993.
Li, T., Shen, H., Zeng, C., Yuan, Q., Zhang, L., 2017b. Point-surface fusion of station measurements and satellite observations for mapping PM2.5 distribution in China: methods and assessment. Atmos. Environ. 152, 477–489.
Li, L., Fang, Y., Wu, J., Wang, J., 2018a. Autoencoder Based Residual Deep Networks for Robust Regression Prediction and Spatiotemporal Estimation. (arXiv preprint arXiv:1812.11262).
Li, T., Shen, H., Yuan, Q., Zhang, L., 2018b. Geographically and Temporally Weighted Neural Networks for Satellite-based Mapping of Ground-level PM2.5. (arXiv preprint arXiv:1809.09860).
Li, X., Liu, S., Li, H., Ma, Y., Wang, J., Zhang, Y., Xu, Z., Xu, T., Song, L., Yang, X., Lu, Z., Wang, Z., Guo, Z., 2018c. Intercomparison of six upscaling evapotranspiration methods: from site to the satellite pixel. J. Geophys. Res. Atmos. 123, 6777–6803.
Li, Q., Yang, T., Zhang, F., Qi, Z., Li, L., 2019. Snow depth reconstruction over last century: trend and distribution in the Tianshan Mountains, China. Glob. Planet. Chang. 173, 73–82.
Liang, S., 2005. Quantitative Remote Sensing of Land Surfaces. John Wiley & Sons 30.
Liang, X.Y., Li, X.Y., Lei, T.W., Wang, W., Gao, Y., 2011. Study of sample temperature compensation in the measurement of soil moisture content. Measurement 44, 2200–2204.
Liao, J., Shen, G., Dong, L., 2013. Biomass estimation of wetland vegetation in Poyang Lake area using ENVISAT advanced synthetic aperture radar data. J. Appl. Remote. Sens. 7, 073579.
Linares-rodriguez, A., Ruiz-arias, J.A., Pozo-vazquez, D., Tovar-pescador, J., 2013. An artificial neural network ensemble model for estimating global solar radiation from Meteosat satellite images. Energy 61, 636–645.
Liou, Y.-A., Liu, S.-F., Wang, W.-J., 2001. Retrieving soil moisture from simulated brightness temperatures by a neural network. IEEE Trans. Geosci. Remote Sens. 39,

1662–1672.
Lipton, Z.C., Berkowitz, J., Elkan, C., 2015. A critical review of recurrent neural networks for sequence learning. (arXiv preprint arXiv:1506.00019v1).
Liu, Y., Wu, L., 2016. Geological disaster recognition on optical remote sensing images using deep learning. Procedia Computer Science 91, 566–575.
Liu, S.-F., Liou, Y.-A., Wang, W.-J., Wigneron, J.-P., Lee, J.-B., 2002. Retrieval of crop biomass and soil moisture from measured 1.4 and 10.65 GHz brightness temperatures. IEEE Trans. Geosci. Remote Sens. 40, 1260–1268.
Liu, M., Liu, X., Li, M., Fang, M., Chi, W., 2010. Neural-network model for estimating leaf chlorophyll concentration in rice under stress from heavy metals using four spectral indices. Biosyst. Eng. 106, 223–233.
Liu, P., Shi, R., Zhang, C., Zeng, Y., Wang, J., Tao, Z., Gao, W., 2017. Integrating multiple vegetation indices via an artificial neural network model for estimating the leaf chlorophyll content of Spartina alterniflora under interspecies competition. Environ. Monit. Assess. 189, 596.
Lu, X., Zhuang, Q., 2010. Evaluating evapotranspiration and water-use efficiency of terrestrial ecosystems in the conterminous United States using MODIS and AmeriFlux data. Remote Sens. Environ. 114, 1924–1939.
Lv, Q., Dou, Y., Niu, X., Xu, J., Xu, J., Xia, F., 2015. Urban land use and land cover classification using remotely sensed SAR data through deep belief networks. Journal of Sensors 2015.
Ma, L., Li, M., Ma, X., Cheng, L., Du, P., Liu, Y., 2017. A review of supervised object-based land-cover image classification. ISPRS J. Photogramm. Remote Sens. 130, 277–293.
Ma, L., Liu, Y., Zhang, X., Ye, Y., Yin, G., Johnson, B.A., 2019. Deep learning in remote sensing applications: a meta-analysis and review. ISPRS J. Photogramm. Remote Sens. 152, 166–177.
Mahdianpari, M., Salehi, B., Rezaee, M., Mohammadimanesh, F., Zhang, Y., 2018. Very deep convolutional neural networks for complex land cover mapping using multispectral remote sensing imagery. Remote Sens. 10, 1119.
Mao, K., Shi, J., Li, Z.-L., Tang, H., 2007. An RM-NN algorithm for retrieving land surface temperature and emissivity from EOS/MODIS data. J. Geophys. Res. Atmos. 112.
Mao, K., Shi, J., Tang, H., Li, Z.L., Wang, X., Chen, K.S., 2008a. A neural network technique for separating land surface emissivity and temperature from ASTER imagery. IEEE Transactions on Geoscience & Remote Sensing 46, 200–208.
Mao, K.B., Tang, H.J., Wang, X.F., Zhou, Q.B., Wang, D.L., 2008b. Near-surface air temperature estimation from ASTER data based on neural network algorithm. Int. J. Remote Sens. 29, 6021–6028.
Mao, K., Zuo, Z., Shen, X., Xu, T., Gao, C., Liu, G., 2018. Retrieval of land-surface temperature from AMSR2 data using a deep dynamic learning neural network. Chin. Geogr. Sci. 28, 1–11.
Marçais, J., de Dreuzy, J.R., 2017. Prospective interest of deep learning for hydrological inference. Groundwater 55, 688–692.
Meng, Q., Zhang, L., Xie, Q., Yao, S., Chen, X., Zhang, Y., 2018. Combined use of GF-3 and Landsat-8 satellite data for soil moisture retrieval over agricultural areas using artificial neural network. Adv. Meteorol. 2018, 1–11.
Musavi, M.T., Miller, R.L., Ressom, H., Natarajan, P., 2002. Neural Network-based Estimation of Chlorophyll-a Concentration in Coastal Waters. International Society for Optics and Photonics, pp. 176–184.
Myint, S.W., Gober, P., Brazel, A., Grossman-Clarke, S., Weng, Q., 2011. Per-pixel vs. object-based classification of urban land cover extraction using high spatial resolution imagery. Remote Sens. Environ. 115, 1145–1161.
Nabavi, S.O., Haimberger, L., Abbasi, R., Samimi, C., 2018. Prediction of aerosol optical depth in West Asia using deterministic models and machine learning algorithms. Aeolian Res. 35, 69–84.
Nagamani, P.V., Chauhan, P., Dwivedi, R.M., 2007. Estimation of chlorophyll-A concentration using an artificial neural network (ANN)-based algorithm with oceansat-I OCM data. Journal of the Indian Society of Remote Sensing 35, 201–207.
Ndikumana, E., Dinh Ho Tong, M., Baghdadi, N., Courault, D., Hossard, L., 2018a. Deep recurrent neural network for agricultural classification using multitemporal SAR Sentinel-1 for Camargue, France. Remote Sens. 10.
Ndikumana, E., Minh, D.H.T., Baghdadi, N., Courault, D., Hossard, L., 2018b. Applying deep learning for agricultural classification using multitemporal SAR Sentinel-1 for Camargue, France. In: Bruzzone, L., Bovolo, F. (Eds.), Image and Signal Processing for Remote Sensing Xxiv. Spie-Int Soc Optical Engineering, Bellingham.
Nijhawan, R., Das, J., Raman, B., 2018. A hybrid of deep learning and hand-crafted features based approach for snow cover mapping. Int. J. Remote Sens. 1–15.
Nock, K., Gilmour, E., Elmore, P., Leadbetter, E., Sweeney, N., Petry, F., 2019. Deep learning on hyperspectral data to obtain water properties and bottom depths. In: International Society for Optics and Photonics, pp. 110180Y.
Notarnicola, C., Angiulli, M., Posa, F., 2008. Soil moisture retrieval from remotely sensed data: neural network approach versus Bayesian method. IEEE Trans. Geosci. Remote Sens. 46, 547–557.
Nussbaumer, E.A., Pinker, R.T., 2012. Estimating surface longwave radiative fluxes from satellites utilizing artificial neural networks. J. Geophys. Res. Atmos. 117.
O'Reilly, J.E., Maritorena, S., Mitchell, B.G., Siegel, D.A., Carder, K.L., Garver, S.A., Kahru, M., McClain, C., 1998. Ocean color chlorophyll algorithms for SeaWiFS. J. Geophys. Res. Oceans 103, 24937–24953.
Overpeck, J.T., Meehl, G.A., Bony, S., Easterling, D.R., 2011. Climate data challenges in the 21st century. Science 331, 700.
Özerdem, M., Acar, E., Ekinci, R., 2017. Soil moisture estimation over vegetated agricultural areas: Tigris Basin, Turkey from Radarsat-2 data by polarimetric decomposition models and a generalized regression neural network. Remote Sens. 9.
Paloscia, S., Pampaloni, P., Pettinato, S., Santi, E., 2008. A comparison of algorithms for retrieving soil moisture from ENVISAT/ASAR images. IEEE Trans. Geosci. Remote Sens. 46, 3274–3284.
Paloscia, S., Pampaloni, P., Pettinato, S., Santi, E., 2010. Generation of soil moisture maps from ENVISAT/ASAR images in mountainous areas: a case study. Int. J. Remote Sens. 31, 2265–2276.
Paloscia, S., Pettinato, S., Santi, E., Notarnicola, C., Pasolli, L., Reppucci, A., 2013. Soil moisture mapping using Sentinel-1 images: algorithm and preliminary validation. Remote Sens. Environ. 134, 234–248.
Panda, S.S., Ames, D.P., Panigrahi, S., 2010. Application of vegetation indices for agricultural crop yield prediction using neural network techniques. Remote Sens. 2, 673–696.
Panda, S., Amatya, D., Jackson, R., Sun, G., Noormets, A., 2018. Automated geospatial models of varying complexities for pine forest evapotranspiration estimation with advanced data mining. Water 10.
Pantazi, X.E., Moshou, D., Alexandridis, T., Whetton, R.L., Mouazen, A.M., 2016. Wheat yield prediction using machine learning and advanced sensing techniques. Comput. Electron. Agric. 121, 57–65.
Park, Y., Kwon, B., Heo, J., Hu, X., Liu, Y., Moon, T., 2020. Estimating PM2.5 concentration of the conterminous United States via interpretable convolutional neural networks. Environ. Pollut. 256, 13395.
Peng, J., Loew, A., Merlin, O., Verhoest, N.E.C., 2017. A review of spatial downscaling of satellite remotely sensed soil moisture. Rev. Geophys. 55, 341–366.
Pierdicca, N., Castracane, P., Pulvirenti, L., 2008. Inversion of electromagnetic models for bare soil parameter estimation from multifrequency polarimetric SAR data. Sensors 8, 8181–8200.
Qin, W., Wang, L., Lin, A., Zhang, M., Bilal, M., 2018. Improving the estimation of daily aerosol optical depth and aerosol radiative effect using an optimized artificial neural network. Remote Sens. 10, 1022.
Qiu, C., Mou, L., Schmitt, M., Zhu, X.X., 2019. Local climate zone-based urban land cover classification from multi-seasonal Sentinel-2 images with a recurrent residual network. ISPRS J. Photogramm. Remote Sens. 154, 151–162.
Quesada-Ruiz, S., Linares-Rodríguez, A., Ruiz-Arias, J.A., Pozo-Vázquez, D., Tovar-Pescador, J., 2015. An advanced ANN-based method to estimate hourly solar radiation from multi-spectral MSG imagery. Sol. Energy 115, 494–504.
Rahimikhoob, A., 2010. Estimation of evapotranspiration based on only air temperature data using artificial neural networks for a subtropical climate in Iran. Theor. Appl. Climatol. 101, 83–91.
Rahimikhoob, A., 2016. Comparison of M5 model tree and artificial neural network's methodologies in modelling daily reference evapotranspiration from NOAA satellite images. Water Resour. Manag. 30, 3063–3075.
Reddy, D.S., Prasad, P.R.C., 2018. Prediction of vegetation dynamics using NDVI time series data and LSTM. Model. Earth Syst. Environ. 4, 409–419.
Reichstein, M., Camps-Valls, G., Stevens, B., Jung, M., Denzler, J., Carvalhais, N., Prabhat, 2019. Deep learning and process understanding for data-driven Earth system science. Nature 566, 195–204.
Ristovski, K., Vucetic, S., Obradovic, Z., 2012. Uncertainty analysis of neural-network-based aerosol retrieval. IEEE Trans. Geosci. Remote Sens. 50, 409–414.
Rodriguez-Fernandez, N., Richaume, P., Aires, F., Prigent, C., Kerr, Y., Kolassa, J., Jimenez, C., Cabot, F., Mahmoodi, A., 2014. Soil moisture retrieval from SMOS observations using neural networks. In: Geoscience and Remote Sensing Symposium (IGARSS), 2014 IEEE International. IEEE, pp. 2431–2434.
Rodriguez-Fernandez, N.J., Aires, F., Richaume, P., Kerr, Y.H., Prigent, C., Kolassa, J., Cabot, F., Jimenez, C., Mahmoodi, A., Drusch, M., 2015. Soil moisture retrieval using neural networks: application to SMOS. IEEE Trans. Geosci. Remote Sens. 53, 5991–6007.
Rodríguez-Fernández, N., Kerr, Y., van der Schalie, R., Al-Yaari, A., Wigneron, J.-P., de Jeu, R., Richaume, P., Dutra, E., Mialon, A., Drusch, M., 2016. Long term global surface soil moisture fields using an SMOS-trained neural network applied to AMSR-E data. Remote Sens. 8.
Rodríguez-Fernández, N.J., de Souza, V., Kerr, Y.H., Richaume, P., Al Bitar, A., 2017a. Soil moisture retrieval using SMOS brightness temperatures and a neural network trained on in situ measurements. In: Geoscience and Remote Sensing Symposium (IGARSS), 2017 IEEE International. IEEE, pp. 1574–1577.
Rodríguez-Fernández, N.J., Muñoz Sabater, J., Richaume, P., Rosnay, P., Kerr, Y.H., Albergel, C., Drusch, M., Mecklenburg, S., 2017b. SMOS near-real-time soil moisture product: processor overview and first validation results. Hydrol. Earth Syst. Sci. 21, 5201–5216.
Sadeghi, M., Asanjan, A.A., Faridzad, M., Nguyen, P., Hsu, K., Sorooshian, S., Braithwaite, D., 2019. PERSIANN-CNN: precipitation estimation from remotely sensed information using artificial neural networks-convolutional neural networks. J. Hydrometeorol. 20, 2273–2289.
Safa, B., Khalili, A., Teshnehlab, M., Liaghat, A., 2014. Artificial Neural Networks (ANNs) application to predict occurrence of phenological stages in wheat using climatic data. International Journal of Agricultural Policy and Research 2, 352–361.
Şahin, M., 2013. Comparison of modelling ANN and ELM to estimate solar radiation over Turkey using NOAA satellite data. Int. J. Remote Sens. 34, 7508–7533.
Şahin, M., Kaya, Y., Uyar, M., 2013. Comparison of ANN and MLR models for estimating solar radiation in Turkey using NOAA/AVHRR data. Adv. Space Res. 51, 891–904.
Şahin, M., Kaya, Y., Uyar, M., Yıldırım, S., 2014. Application of extreme learning machine for estimating solar radiation from satellite data. Int. J. Energy Res. 38, 205–212.
Santi, E., Pettinato, S., Paloscia, S., Pampaloni, P., Macelloni, G., Brogioni, M., 2012. An algorithm for generating soil moisture and snow depth maps from microwave spaceborne radiometers: HydroAlgo. Hydrol. Earth Syst. Sci. 16, 3659–3676.
Santi, E., Paloscia, S., Pettinato, S., Fontanelli, G., 2014. A prototype ann based algorithm for the soil moisture retrieval from l-band in view of the incoming SMAP mission. In: Microwave Radiometry and Remote Sensing of the Environment (MicroRad), 2014 13th Specialist Meeting on. IEEE, pp. 5–9.
Santi, E., Paloscia, S., Pettinato, S., Brocca, L., Ciabatta, L., 2016. Robust assessment of an operational algorithm for the retrieval of soil moisture from AMSR-E data in central

Italy. IEEE Journal of Selected Topics in Applied Earth Observations and Remote Sensing 9, 2478–2492.
Santi, E., Paloscia, S., Pettinato, S., Brocca, L., Ciabatta, L., Entekhabi, D., 2018a. Integration of microwave data from SMAP and AMSR2 for soil moisture monitoring in Italy. Remote Sens. Environ. 212, 21–30.
Santi, E., Paloscia, S., Pettinato, S., Brocca, L., Ciabatta, L., Entekhabi, D., 2018b. On the synergy of SMAP, AMSR2 AND SENTINEL-1 for retrieving soil moisture. Int. J. Appl. Earth Obs. Geoinf. 65, 114–123.
Savin, I.Y., Stathakis, D., Negre, T., Isaev, V.A., 2007. Prediction of crop yields with the use of neural networks. Russ. Agric. Sci. 33, 361–363.
Schoof, J.T., Pryor, S.C., 2001. Downscaling temperature and precipitation: a comparison of regression-based methods and artificial neural networks. Int. J. Climatol. 21, 773–790.
Schütt, K.T., Arbabzadah, F., Chmiela, S., Müller, K.R., Tkatchenko, A., 2017. Quantum-chemical insights from deep tensor neural networks. Nat. Commun. 8, 13890.
Scott, G.J., England, M.R., Starms, W.A., Marcum, R.A., Davis, C.H., 2017a. Training deep convolutional neural networks for land-cover classification of high-resolution imagery. IEEE Geosci. Remote Sens. Lett. 14, 549–553.
Scott, G.J., Marcum, R.A., Davis, C.H., Nivin, T.W., 2017b. Fusion of deep convolutional neural networks for land cover classification of high-resolution imagery. IEEE Geosci. Remote Sens. Lett. 14, 1638–1642.
Scott, G.J., Hagan, K.C., Marcum, R.A., Hurt, J.A., Anderson, D.T., Davis, C.H., 2018. Enhanced fusion of deep neural networks for classification of benchmark high-resolution image data sets. IEEE Geosci. Remote Sens. Lett. 15, 1451–1455.
Şenkal, O., 2010. Modeling of solar radiation using remote sensing and artificial neural network in Turkey. Energy 35, 4795–4801.
Şenkal, O., Kuleli, T., 2009. Estimation of solar radiation over Turkey using artificial neural network and satellite data. Appl. Energy 86, 1222–1228.
Shaker, A., Yan, W.Y., LaRocque, P.E., 2019. Automatic land-water classification using multispectral airborne LiDAR data for near-shore and river environments. ISPRS J. Photogramm. Remote Sens. 152, 94–108.
Shen, C., 2018. Deep learning: a next-generation big-data approach for hydrology. EOS 99, 1.
Shen, H., Li, X., Cheng, Q., Zeng, C., Yang, G., Li, H., Zhang, L., 2015. Missing information reconstruction of remote sensing data: a technical review. IEEE Geoscience and Remote Sensing Magazine 3, 61–85.
Shen, H., Meng, X., Zhang, L., 2016. An integrated framework for the spatio-temporal-spectral fusion of remote sensing images. IEEE Trans. Geosci. Remote Sens. 54, 7135–7148.
Shen, C., Laloy, E., Elshorbagy, A., Albert, A., Bales, J., Chang, F.-J., Ganguly, S., Hsu, K.-L., Kifer, D., Fang, Z., 2018a. HESS opinions: incubating deep-learning-powered hydrologic science advances as a community. Hydrol. Earth Syst. Sci. 22.
Shen, H., Li, T., Yuan, Q., Zhang, L., 2018b. Estimating regional ground-level PM2.5 directly from satellite top-of-atmosphere reflectance using deep belief networks. J. Geophys. Res. Atmos. 123, 13,875–813,886.
Shen, H., Jiang, Y., Li, T., Cheng, Q., Zeng, C., Zhang, L., 2020. Deep Learning-based Air Temperature Mapping by Fusing Remote Sensing, Station, Simulation and Socioeconomic Data. (arXiv:2001.04650).
Shwetha, H.R., Kumar, D.N., 2016. Prediction of high spatio-temporal resolution land surface temperature under cloudy conditions using microwave vegetation index and ANN. ISPRS J. Photogramm. Remote Sens. 117, 40–55.
Smith, B.A., Mcclendon, R.W., Hoogenboom, G., 2006. Improving air temperature prediction with artificial neural networks. Int. J. Comput. Intell. 3, 179–186.
Snauffer, A.M., Hsieh, W.W., Cannon, A.J., Schnorbus, M.A., 2018. Improving gridded snow water equivalent products in British Columbia, Canada: multi-source data fusion by neural network models. Cryosphere 12, 891–905.
Sobayo, R., Wu, H.-H., Ray, R., Qian, L., 2018. Integration of convolutional neural network and thermal images into soil moisture estimation. In: 2018 1st International Conference on Data Intelligence and Security (ICDIS), pp. 207–210.
Song, X., Zhang, G., Liu, F., Li, D., Zhao, Y., Yang, J., 2016. Modeling spatio-temporal distribution of soil moisture by deep learning-based cellular automata model. Journal of Arid Land 8, 734–748.
Srivastava, P.K., Han, D., Ramirez, M.R., Islam, T., 2013. Machine learning techniques for downscaling SMOS satellite soil moisture using MODIS land surface temperature for hydrological application. Water Resour. Manag. 27, 3127–3144.
Sudheer, K., Gosain, A., Ramasastri, K., 2003. Estimating actual evapotranspiration from limited climatic data using neural computing technique. J. Irrig. Drain. Eng. 129, 214–218.
Sun, Y., Zeng, Q., Geng, B., Lin, X., Sude, B., Chen, L., 2019. Deep learning architecture for estimating hourly ground-level PM2.5 using satellite remote sensing. IEEE Geosci. Remote Sens. Lett. 16, 1343–1347.
Tan, J., NourEldeen, N., Mao, K., Shi, J., Li, Z., Xu, T., Yuan, Z., 2019. Deep learning convolutional neural network for the retrieval of land surface temperature from AMSR2 data in China. Sensors 19, 2987.
Tanaka, A., Kishino, M., Doerffer, R., Schiller, H., Oishi, T., Kubota, T., 2004. Development of a neural network algorithm for retrieving concentrations of chlorophyll, suspended matter and yellow substance from radiance data of the ocean color and temperature scanner. J. Oceanogr. 60, 519–530.
Tanikawa, T., Li, W., Kuchiki, K., Aoki, T., Hori, M., Stamnes, K., 2015. Retrieval of snow physical parameters by neural networks and optimal estimation: case study for ground-based spectral radiometer system. Opt. Express 23, A1442–A1462.
Tao, Y., Gao, X., Hsu, K., Sorooshian, S., Ihler, A., 2016a. A deep neural network modeling framework to reduce bias in satellite precipitation products. J. Hydrometeorol. 17, 931–945.
Tao, Y., Gao, X., Ihler, A., Hsu, K., Sorooshian, S., 2016b. Deep Neural Networks for Precipitation Estimation From Remotely Sensed Information. IEEE, pp. 1349–1355.
Tao, Y., Gao, X., Ihler, A., Sorooshian, S., Hsu, K., 2017. Precipitation identification with bispectral satellite information using deep learning approaches. J. Hydrometeorol. 18, 1271–1283.
Tao, Y., Hsu, K., Ihler, A., Gao, X., Sorooshian, S., 2018. A two-stage deep neural network framework for precipitation estimation from bispectral satellite information. J. Hydrometeorol. 19, 393–408.
Tapiador, F.J., Kidd, C., Hsu, K.L., Marzano, F., 2004. Neural networks in satellite rainfall estimation. Meteorol. Appl. 11, 83–91.
Taylor, M., Kazadzis, S., Tsekeri, A., Gkikas, A., Amiridis, V., 2014. Satellite retrieval of aerosol microphysical and optical parameters using neural networks: a new methodology applied to the Sahara desert dust peak. Atmospheric Measurement Techniques 7, 3151–3175.
Tedesco, M., Pulliainen, J., Takala, M., Hallikainen, M., Pampaloni, P., 2004. Artificial neural network-based techniques for the retrieval of SWE and snow depth from SSM/I data. Remote Sens. Environ. 90, 76–85.
Tiwari, P., Shukla, P., 2019. Artificial Neural Network-based Crop Yield Prediction Using NDVI, SPI, VCI Feature Vectors. 933 Springer.
Tong, X.-Y., Xia, G.-S., Lu, Q., Shen, H., Li, S., You, S., Zhang, L., 2020. Land-cover classification with high-resolution remote sensing images using transferable deep models. Remote Sens. Environ. 237, 111322.
Tracewski, L., Bastin, L., Fonte, C.C., 2017. Repurposing a deep learning network to filter and classify volunteered photographs for land cover and land use characterization. Geo-spatial Information Science 20, 252–268.
Trajkovic, S., 2005. Temperature-based approaches for estimating reference evapotranspiration. J. Irrig. Drain. Eng. 131, 316–323.
Trajkovic, S., Stankovic, M., Todorovic, B., 2000. Estimation of FAO Blaney-Criddle b factor by RBF network. J. Irrig. Drain. Eng. 126, 268–270.
Trajkovic, S., Todorovic, B., Stankovic, M., 2003. Forecasting of reference evapotranspiration by artificial neural networks. J. Irrig. Drain. Eng. 129, 454–457.
Trombetti, M., Riano, D., Rubio, M., Cheng, Y., Ustin, S., 2008. Multi-temporal vegetation canopy water content retrieval and interpretation using artificial neural networks for the continental USA. Remote Sens. Environ. 112, 203–215.
Ustaoglu, B., Cigizoglu, H.K., Karaca, M., 2008. Forecast of daily mean, maximum and minimum temperature time series by three artificial neural network methods. Meteorol. Appl. 15, 431–445.
Venkateshwarlu, C., Gopal, K., Prakash, A., 2004. Neural networks in land surface temperature mapping in urban areas from thermal infrared data. International Geoscience and Remote Sensing Symposium (IGARSS) 3 (1589-1590b).
Vucetic, S., Han, B., Mi, W., Li, Z., Obradovic, Z., 2008. A data-mining approach for the validation of aerosol retrievals. IEEE Geosci. Remote Sens. Lett. 5, 113–117.
Wagle, P., Xiao, X., Gowda, P., Basara, J., Brunsell, N., Steiner, J., K.C, A., 2017. Analysis and estimation of tallgrass prairie evapotranspiration in the central United States. Agric. For. Meteorol. 232, 35–47.
Wang, W., Liang, S., Augustine, J.A., 2009. Estimating high spatial resolution clear-sky land surface upwelling longwave radiation from MODIS data. IEEE Trans. Geosci. Remote Sens. 47, 1559–1570.
Wang, T., Yan, G., Chen, L., 2012. Consistent retrieval methods to estimate land surface shortwave and longwave radiative flux components under clear-sky conditions. Remote Sens. Environ. 124, 61–71.
Wang, N., Li, Z., Tang, B., Zeng, F., Li, C., 2013. Retrieval of atmospheric and land surface parameters from satellite-based thermal infrared hyperspectral data using a neural network technique. Int. J. Remote Sens. 34, 3485–3502.
Wang, A.X., Tran, C., Desai, N., Lobell, D., Ermon, S., 2018. Deep transfer learning for crop yield prediction with remote sensing data. In: ACM SIGCAS Conference on Computing and Sustainable Societies (COMPASS), pp. 1–5.
Wang, T., Liang, J., Liu, X., 2019a. Soil moisture retrieval algorithm based on TFA and CNN. IEEE Access 7, 597–604.
Wang, W., Zhao, S., Jiao, L., Taylor, M., Zhang, B., Xu, G., Hou, H., 2019b. Estimation of PM2.5 concentrations in China using a spatial back propagation neural network. Sci. Rep. 9, 13788.
Wei, Y., Zheng, Y., Yang, Q., 2016. Transfer knowledge between cities. In: Proceedings of the 22nd ACM SIGKDD International Conference on Knowledge Discovery and Data Mining. ACM, San Francisco, California, USA, pp. 1905–1914.
Wen, C., Liu, S., Yao, X., Peng, L., Li, X., Hu, Y., Chi, T., 2019. A novel spatiotemporal convolutional long short-term neural network for air pollution prediction. Sci. Total Environ. 654, 1091–1099.
Wolanin, A., Camps-Valls, G., Gómez-Chova, L., Mateo-Garcí, G., Tol, C., Zhang, Y., Guanter, L., 2019. Estimating crop primary productivity with Sentinel-2 and Landsat 8 using machine learning methods trained with radiative transfer simulations. Remote Sens. Environ. 225 (7).
Wu, Y., Guo, J., Zhang, X., Tian, X., Zhang, J., Wang, Y., Duan, J., Li, X., 2012. Synergy of satellite and ground based observations in estimation of particulate matter in eastern China. Sci. Total Environ. 433, 20–30.
Wu, H., Liu, B.Z., Su, W.H., Zhang, W.C., Sun, J.G., 2016. Deep filter banks for land-use scene classification. IEEE Geosci. Remote Sens. Lett. 13, 1895–1899.
Wu, P., Yin, Z., Yang, H., Wu, Y., Ma, X., 2019. Reconstructing geostationary satellite land surface temperature imagery based on a multiscale feature connected convolutional neural network. Remote Sens. 11, 300.
Xiao, Z., Liang, S., Wang, J., Chen, P., Yin, X., Zhang, L., Song, J., 2014. Use of general regression neural networks for generating the GLASS leaf area index product from time-series MODIS surface reflectance. IEEE Trans. Geosci. Remote Sens. 52.
Xiao, Z., Liang, S., Wang, J., Xiang, Y., Zhao, X., Song, J., 2016. Long-time-series global land surface satellite leaf area index product derived from MODIS and AVHRR surface reflectance. IEEE Trans. Geosci. Remote Sens. 54, 15.
Xiao, X., Zhang, T., Zhong, X., Shao, W., Li, X., 2018. Support vector regression snow-depth retrieval algorithm using passive microwave remote sensing data. Remote

Sens. Environ. 210, 48–64.
Xie, Y., Sha, Z., Yu, M., Bai, Y., Zhang, L., 2009. A comparison of two models with Landsat data for estimating above ground grassland biomass in Inner Mongolia, China. Ecol. Model. 220, 1810–1818.
Xing, C., Chen, N., Zhang, X., Gong, J., 2017. A machine learning based reconstruction method for satellite remote sensing of soil moisture images with in situ observations. Remote Sens. 9.
Xing, H.F., Meng, Y., Wang, Z.X., Fan, K.X., Hou, D.Y., 2018. Exploring geo-tagged photos for land cover validation with deep learning. ISPRS J. Photogramm. Remote Sens. 141, 237–251.
Xu, G., Zhu, X., Fu, D.J., Dong, J.W., Xiao, X.M., 2017. Automatic land cover classification of geo-tagged field photos by deep learning. Environ. Model. Softw. 91, 127–134.
Xu, H., Yuan, Q., Li, T., Shen, H., Zhang, L., Jiang, H., 2018a. Quality improvement of satellite soil moisture products by fusing with in-situ measurements and GNSS-R estimates in the western continental U.S. Remote Sens. 10.
Xu, T., Guo, Z., Liu, S., He, X., Meng, Y., Xu, Z., Xia, Y., Xiao, J., Zhang, Y., Ma, Y., 2018b. Evaluating different machine learning methods for upscaling evapotranspiration from flux towers to the regional scale. J. Geophys. Res. Atmos. 123, 8674–8690.
Yadav, A.K., Chandel, S.S., 2014. Solar radiation prediction using artificial neural network techniques: a review. Renew. Sust. Energ. Rev. 33, 772–781.
Yan, G., Mas, J.F., Maathuis, B.H.P., Xiangmin, Z., Van Dijk, P.M., 2006. Comparison of pixel-based and object-oriented image classification approaches—a case study in a coal fire area, Wuda, Inner Mongolia, China. Int. J. Remote Sens. 27, 4039–4055.
Yang, X.-h., Huang, J.-f., Wang, J.-w., Wang, X.-z., Liu, Z.-y., 2007. Estimation of vegetation biophysical parameters by remote sensing using radial basis function neural network. Journal of Zhejiang University-Science A 8, 883–895.
Yang, G., Pu, R., Huang, W., Wang, J., Zhao, C., 2010. A novel method to estimate subpixel temperature by fusing solar-reflective and thermal-infrared remote-sensing data with an artificial neural network. IEEE Transactions on Geoscience & Remote Sensing 48, 2170–2178.
Yang, Y.J., Zhu, J.H., Zhao, C.J., Liu, S.Y., Tong, X.Q., 2011. The spatial continuity study of NDVI based on Kriging and BPNN algorithm. Math. Comput. Model. 54, 1138–1144.
Yang, X., Xu, B., Yunxiang, J., Jinya, L., Zhu, X., 2012. On Grass Yield Remote Sensing Estimation Models of China's Northern Farming-Pastoral Ecotone. In: Lee, G. (Ed.), Advances in Computational Environment Science. Advances in Intelligent and Soft Computing. 142 Springer, Berlin, Heidelberg.
Yang, J., Gong, P., Fu, R., Zhang, M., Chen, J., Liang, S., Xu, B., Shi, J., Dickinson, R., 2013. The role of satellite remote sensing in climate change studies. Nat. Clim. Chang. 3, 875–883.
Yang, G., Shen, H., Zhang, L., He, Z., Li, X., 2015. A moving weighted harmonic analysis method for reconstructing high-quality SPOT VEGETATION NDVI time-series data. IEEE Trans. Geosci. Remote Sens. 53, 6008–6021.
Yang, L., Jia, K., Liang, S., Wei, X., Yao, Y., Zhang, X., 2017. A Robust Algorithm for Estimating Surface Fractional Vegetation Cover from Landsat Data. Remote Sens. 9, 857.
Yang, Y., Dong, J., Sun, X., Lima, E., Mu, Q., Wang, X., 2018. A CFCC-LSTM model for sea surface temperature prediction. IEEE Geosci. Remote Sens. Lett. 15, 207–211.
Yeom, J.-M., Park, S., Chae, T., Kim, J.-Y., Lee, C.S., 2019. Spatial assessment of solar radiation by machine learning and deep neural network models using data provided by the COMS MI geostationary satellite: a case study in South Korea. Sensors 19, 2082.
You, J., Li, X., Low, M., Lobell, D., Ermon, S., 2017. Deep Gaussian process for crop yield prediction based on remote sensing data. In: Proceedings of the Thirty-first AAAI Conference on Artificial Intelligence.
Yuan, Y., Jia, K.B., 2015. A Water Quality Assessment Method Based on Sparse Autoencoder. Ieee, New York.
Yuan, Q., Xu, H., Li, T., Shen, H., Zhang, L., 2020. Estimating surface soil moisture from satellite observations using a generalized regression neural network trained on sparse ground-based measurements in the continental U.S. J. Hydrol. 580, 124351.
Zang, L., Mao, F., Guo, J., Gong, W., Wang, W., Pan, Z., 2018. Estimating hourly PM1 concentrations from Himawari-8 aerosol optical depth in China. Environ. Pollut. 241, 654–663.
Zang, L., Mao, F., Guo, J., Wang, W., Pan, Z., Shen, H., Zhu, B., Wang, Z., 2019. Estimation of spatiotemporal PM1.0 distributions in China by combining PM2.5 observations with satellite aerosol optical depth. Sci. Total Environ. 658, 1256–1264.
Zeiler, M.D., Fergus, R., 2014. Visualizing and understanding convolutional networks. In: European Conference on Computer Vision. Springer, pp. 818–833.
Zeng, C., Shen, H., Zhang, L., 2013. Recovering missing pixels for Landsat ETM+ SLC-off imagery using multi-temporal regression analysis and a regularization method. Remote Sens. Environ. 131, 182–194.
Zeng, C., Long, D., Shen, H., Wu, P., Cui, Y., Hong, Y., 2018. A two-step framework for reconstructing remotely sensed land surface temperatures contaminated by cloud. ISPRS J. Photogramm. Remote Sens. 141, 30–45.
Zhan, W., Chen, Y., Zhou, J., Wang, J., Liu, W., Voogt, J., Zhu, X., 2013. Disaggregation of remotely sensed land surface temperature: literature survey, taxonomy, issues, and caveats. Remote Sens. Environ. 131, 119–139.
Zhang, L., Ma, W., Zhang, D., 2016a. Stacked sparse autoencoder in PolSAR data classification using local spatial information. IEEE Geosci. Remote Sens. Lett. 13, 1359–1363.
Zhang, L., Zhang, L., Du, B., 2016b. Deep learning for remote sensing data: a technical tutorial on the state of the art. IEEE Geoscience and Remote Sensing Magazine 4, 22–40.
Zhang, D., Zhang, W., Huang, W., Hong, Z., Meng, L., 2017a. Upscaling of surface soil moisture using a deep learning model with VIIRS RDR. ISPRS Int. J. Geo Inf. 6, 130.
Zhang, J., Zhao, L., Deng, S., Xu, W., Zhang, Y., 2017b. A critical review of the models used to estimate solar radiation. Renew. Sust. Energ. Rev. 70, 314–329.
Zhang, C., Pan, X., Li, H., Gardiner, A., Sargent, I., Hare, J., Atkinson, P.M., 2018a. A hybrid MLP-CNN classifier for very fine resolution remotely sensed image classification. ISPRS J. Photogramm. Remote Sens. 140, 133–144.
Zhang, C., Sargent, I., Pan, X., Li, H., Gardiner, A., Hare, J., Atkinson, P.M., 2018b. An object-based convolutional neural network (OCNN) for urban land use classification. Remote Sens. Environ. 216, 57–70.
Zhang, Q., Yuan, Q., Zeng, C., Li, X., Wei, Y., 2018c. Missing data reconstruction in remote sensing image with a unified spatial–temporal–spectral deep convolutional neural network. IEEE Trans. Geosci. Remote Sens. 56, 4274–4288.
Zhang, X., Zhang, Q., Zhang, G., Nie, Z., Gui, Z., Que, H., 2018d. A novel hybrid data-driven model for daily land surface temperature forecasting using long short-term memory neural network based on ensemble empirical mode decomposition. Int. J. Environ. Res. Public Health 15, 1032.
Zhang, Z., Gong, Y., Wang, Z., 2018e. Accessible remote sensing data based reference evapotranspiration estimation modelling. Agric. Water Manag. 210, 59–69.
Zhang, C., Sargent, I., Pan, X., Li, H., Gardiner, A., Hare, J., Atkinson, P.M., 2019. Joint deep learning for land cover and land use classification. Remote Sens. Environ. 221, 173–187.
Zhao, W., Du, S., 2016. Learning multiscale and deep representations for classifying remotely sensed imagery. ISPRS J. Photogramm. Remote Sens. 113, 155–165.
Zhao, D., Zhang, W., Shijin, X., 2007. A neural network algorithm to retrieve nearsurface air temperature from landsat ETM+ imagery over the Hanjiang River Basin, China. In: Geoscience and Remote Sensing Symposium, 2007. IGARSS 2007. IEEE International. IEEE, pp. 1705–1708.
Zhao, W., Guo, Z., Yue, J., Zhang, X., Luo, L., 2015. On combining multiscale deep learning features for the classification of hyperspectral remote sensing imagery. Int. J. Remote Sens. 36, 3368–3379.
Zhao, B., Huang, B., Zhong, Y., 2017. Transfer learning with fully pretrained deep convolution networks for land-use classification. IEEE Geoscience Remote Sensing Letters 14, 1436–1440.
Zhao, H., Chen, Z., Jiang, H., Jing, W., Sun, L., Feng, M., 2019. Evaluation of three deep learning models for early crop classification using Sentinel-1A imagery time series-a case study in Zhanjiang, China. Remote Sens. 11.
Zhong, P., Gong, Z., Li, S., Schönlieb, C., 2017. Learning to diversify deep belief networks for hyperspectral image classification. IEEE Trans. Geosci. Remote Sens. 55, 3516–3530.
Zhu, X.X., Tuia, D., Mou, L., Xia, G.-S., Zhang, L., Xu, F., Fraundorfer, F., 2017. Deep learning in remote sensing: a comprehensive review and list of resources. IEEE Geoscience and Remote Sensing Magazine 5, 8–36.